


ORIGINAL ARTICLE OPEN ACCESS

Flood Susceptibility for Storage Dams Locations to Reduce the Risk of Flash Floods and to Harvest Rainfall Utilizing a GIS Spatial Distribution Model and the Analytical Hierarchy Approach

Mahmoud M. Afify¹ | Ismail Abd-Elaty²  | Amir S. Ibrahim¹  | Islam S. Al Zayed³ | Ashraf Ahmed⁴  | Fahmy S. Abdelhaleem¹

¹Civil Engineering Department, Benha Faculty of Engineering, Benha University, Benha, Egypt | ²Department of Water and Water Structures Engineering, Faculty of Engineering, Zagazig University, Zagazig, Egypt | ³Technical Office, National Water Research Centre, Cairo, Egypt | ⁴Department of Civil and Environmental Engineering, Brunel University London, Uxbridge, UK

Correspondence: Ismail Abd-Elaty (eng_abdelaty2006@yahoo.com; eng_abdelaty@zu.edu.eg) | Ashraf Ahmed (ashraf.ahmed@brunel.ac.uk)

Received: 13 March 2025 | **Revised:** 24 September 2025 | **Accepted:** 15 October 2025

Keywords: analytical hierarchy approach | dams | flash flood | GIS | multi-criteria decision-making | Wadi ked

ABSTRACT

Flooding is a natural calamity that causes widespread devastation, including severe infrastructure destruction, significant economic consequences, and social disturbances around the world, particularly in the Sinai region. Wadi Ked is one of Sinai, Egypt's, most vulnerable districts to flood hazards, and it is the location used for this study. This study aims to create a map of flood-prone areas in Wadi Ked by combining Geographic Information System (GIS) technology and multi-criteria decision-making (MCDM) techniques, utilizing the Analytical Hierarchy Process (AHP) methodology. To achieve the study's goal, flood-related factors such as elevation, slope, distance to roads, distance from streams, annual rainfall, drainage density, topographic wetness index, land use and land cover, normalized difference vegetation index, soil type, and curvature were weighted and overlaid. The results show that 26.91% of the areas studied have a low sensitivity to flooding, whereas roughly 73.09% of the area is moderately to very highly vulnerable to flooding. The study proposed a dam with a height of 30 m, a width of 0.416 km, and a lake capacity of 31.74 million cubic meters (MCM). The surface runoff volumes from 50- and 100-year storms in sub-basins 1–5 are 23.07 MCM and 29.66 MCM, respectively. Model validation was performed by comparing susceptibility maps generated from literature-based and expert-based AHP weights, revealing a 98% spatial agreement and a Kappa coefficient of 0.995, confirming the model's robustness. This study offers value to decision-makers and planners by utilizing morphometric properties and flash flood risk maps to identify suitable locations for dams.

Abbreviations: AHP, analytical hierarchy process; AUC, curves and area under the curve; C, celices; C, curvature; CI, consistency index; CN, curve number; CR, consistency ratio; DD, drainage density; DEM, digital elevation model; DR, distance to roads; DS, distance to streams; E, elevation; FAO, Food and Agriculture Organization of the United Nations; GCS, geographic coordinate systems; GIS, geographic information system; HEC-HMS, hydrologic engineering center–hydrologic modeling system; HEC-RAS, Hydrologic Engineering Center's River Analysis System; IDW, inverse distance weighted; LULC, land use and land cover; MCDM, multi-criteria decision-making; MCM, million cubic meters; NDVI, Normalized Difference Vegetation Index; OSM, open street map; PhD, doctor of philosophy; R, rainfall; RI, random index; ROC, receiver operating characteristic; S, slope; SCS-CN, soil conservation service curve number; ST, soil type; TWI, Topographic Wetness Index; US, United States; UTM, Universal Transverse Mercator; WGS, World Geodetic System; WRRRI, Water Resources Research Institute.

This is an open access article under the terms of the [Creative Commons Attribution](https://creativecommons.org/licenses/by/4.0/) License, which permits use, distribution and reproduction in any medium, provided the original work is properly cited.

© 2025 The Author(s). *Journal of Flood Risk Management* published by Chartered Institution of Water and Environmental Management and John Wiley & Sons Ltd.

1 | Introduction

Flooding is a natural disaster that results in extensive damage, including significant harm to infrastructure, substantial economic losses, and social disruptions worldwide (Dang and Kumar 2017; Das and Gupta 2021; Farhadi and Najafzadeh 2021; Hong, Panahi, et al. 2018; Hong, Tsangaratos, et al. 2018). In recent years, many countries worldwide have experienced an increase in flood-related destruction, attributed to climate change and environmental degradation resulting from inadequate land-use management practices (Das and Gupta 2021; Hagos et al. 2022; Kanani-Sadat et al. 2019; Ozkan and Tarhan 2016). In the Sinai region, flooding stands out as a major natural hazard that inflicts significant harm on lives, livelihoods, and property across various areas of the region. Flooding in dry areas is primarily linked to extended periods of intense rainfall and the terrain of the elevated areas and low-lying plains, which feature natural drainage systems formed by major river basins. The objective of this study was to locate and chart flood-prone areas in Wadi Ked. Despite the district's recognition as a flood-prone area in South Sinai, no prior studies have been conducted to identify and map these areas. Effective management of flood risk relies on acquiring knowledge about the risk and likelihood of flood occurrences (Binns 2022). Recently, mapping potential flood risk areas has emerged as a crucial strategic element in the effective management, reduction, and mitigation of potential flood hazards. These maps can provide residents and stakeholders with valuable information about areas susceptible to flooding (Abdelkarim et al. 2020; Rahmati et al. 2015). Previous researchers have devised various methods and models to study and map flood hazards. Abd-Elaty et al. (2024) applied rainwater harvesting in combination with the managed aquifer recharge technique to develop the integrated water resources management in arid and semi-arid regions.

Recently, the combined application of geospatial technologies, such as Geographic Information Systems (GIS) and remote sensing, with other methods and models has emerged as the predominant approach for analyzing flood hazards. Ali et al. (2020) employed GIS integration, a multi-criteria decision-making (MCDM) approach, bivariate statistics (frequency ratio and statistical index), and logistic regression to identify flood-prone areas within the Topľa River Basin in Slovakia. Demir and Kisi (2016) utilized GIS and the Hydrologic Engineering Centres River Analysis System (HEC-RAS) to generate a flood hazard map for the Mert River basin in Turkey. Hong, Panahi, et al. (2018); Hong, Tsangaratos, et al. (2018) employed the integration of fuzzy weight of evidence, logistic regression, random forest, and support vector machines with GIS to generate a flood susceptibility map of Poyang County in China. Razavi-Termeh et al. (2018) combined adaptive neuro-fuzzy inference systems with metaheuristic algorithms and GIS to map flood hazards in the Jahrom basin located in the Fars Province of Iran. Tehrany et al. (2017) forecasted flood-prone areas in Xing Guo, situated in southern Jiangxi Province, China, by combining GIS with standalone frequency ratio, weight of evidence, and logistic regression methods. Zhao et al. (2018) utilized the random forest model to create a map depicting the susceptibility to flooding in mountainous regions of China.

Many studies have used GIS-based MCDM and Analytic Hierarchy Process (AHP) to map flood-prone areas. Abdelkarim et al. (2020) employed the AHP method and a GIS-based MCDM approach to evaluate flood risk locations along the Al-Shamal Train Pathway in the Al-Qurayyat Region, Kingdom of Saudi Arabia. Aydin and Birincioğlu (2022) employed a GIS-based analytical hierarchy to evaluate flood risk zones in Bitlis Province, Turkey, incorporating nine elements that control floods. Desalegn and Mulu (2021) used a combination of GIS-based MCDM and AHP to assess and map flood vulnerability in the Fetam watershed, situated in the upper Abay basin of Ethiopia. Hagos et al. (2022) employed GIS-MCDM and AHP to identify flood-prone locations in Ethiopia's Upper Awash River Basin. MCDM is a valuable tool for evaluating complicated decision-making situations, such as identifying and mapping flood-prone areas based on several criteria and data (Abdelkarim et al. 2020; Ali et al. 2020), and AHP is the most often used method for multi-criteria decision-making (Abdelkarim et al. 2020; Das and Gupta 2021). Ibrahim et al. (2023) applied the GIS and the basin's morphometric characteristics to determine the most economical sites for storage dams in Wadi Tayyibah, south Sinai, Egypt. In sub-basins (1) and (4), where the runoff volumes reached 3.13 MCM and 5.56 MCM during the return period of 100, respectively, the study indicated that dams (#3) and (#7) were the optimal dam placements. Decision-makers can utilize the morphometric characteristics of the current study to inform rainwater harvesting and flash flood hazard maps, thereby determining the optimal location for storage dam investment. The literature review was expanded to incorporate recent (2021–2024) flood susceptibility studies that utilized advanced GIS–MCDM techniques in arid and semi-arid regions. Zhran et al. (2024), who conducted their study in the Damietta branch, Egypt, applied a GIS–AHP framework validated using receiver operating characteristic (ROC) curves and area under the curve (AUC) analysis, reporting an AUC value of 0.741, which indicates moderate predictive performance. In Ghanem and Zaifoglu (2024), the authors successfully combined Fuzzy–AHP with the frequency ratio method to enhance classification accuracy and model robustness. Ali et al. (2023) applied a hybrid Fuzzy–AHP model, achieving a high AUC of 97%, confirming the strength of combining fuzzy logic with statistical methods.

Similar integrated methodologies have been employed in Saudi Arabia using Fuzzy-AHP within GIS environments to map flood susceptibility more accurately (Bokhari et al. 2024). In Algeria, recent studies including Rebouh et al. (2024) and Berghout (2025) implemented comparable approaches, emphasizing the effectiveness of hybrid and expert-based MCDM models in data-scarce and topographically complex terrains.

Collectively, these studies underscore the growing reliance on modern AHP-based frameworks, often enhanced with fuzzy logic, statistical validation, and multi-source geospatial platforms, thereby reinforcing the methodological foundation and contemporary relevance of the present study.

Moreover, despite having the Nile River, Egypt faces water scarcity issues. The identification of suitable dam locations is based on the Flood Susceptibility Map of Wadi Ked. The study region holds strategic significance for Egypt, underscoring the

importance of finding innovative ways to harness floodwaters in the Wadi Ked. Given the hydrological and climatic characteristics of Wadi Ked, selecting an appropriate method for assessing flood susceptibility is crucial. The AHP integrated within the MCDM framework, was selected for this study due to its proven adaptability in data-scarce environments. Arid regions such as South Sinai often lack dense rainfall gauges or high-resolution hydrological datasets, which limit the feasibility of purely data-driven models. AHP enables the systematic integration of limited spatial data with expert knowledge, providing a flexible yet robust alternative for flood risk mapping. The AHP-MCDM approach was chosen based on three primary considerations. First, data scarcity: Wadi Ked suffers from limited hydrological observations, making traditional flood modeling approaches difficult to apply. Second, regional suitability: numerous studies in arid and semi-arid regions have demonstrated the success of AHP in flood hazard assessment (e.g., Alarifi et al. 2022; Elsadek and Almaliki 2024). Finally, AHP provides a transparent, scalable, and easily interpretable decision-making structure, making it ideal for local planners and stakeholders to replicate across other catchments in Sinai and similar dryland environments.

In the study area, 11 factors affecting flood occurrences were identified. These factors include Elevation (E), Slope (S), Rainfall (R), Distance to streams (DS), Distance to Roads (DR), Drainage Density (DD), Topographic Wetness Index (TWI), Land Use and Land Cover (LULC), Normalized Difference Vegetation Index (NDVI), Soil Type (ST), and Curvature (C). This study was conducted to identify and map flood-prone areas within the district, recognizing the importance of such efforts for residents and decision-makers seeking to mitigate and manage flood risks effectively.

Although several studies have employed GIS and MCDM techniques for flood susceptibility mapping in various parts of Egypt and the Middle East, to the best of our knowledge, no prior research has applied an integrated GIS-AHP approach to assess flood risk in the Wadi Ked basin. Furthermore, this study is the first to directly link spatial flood susceptibility analysis with the siting of rainwater harvesting structures, specifically identifying suitable dam locations based on runoff dynamics. This dual contribution enhances both the methodological and practical relevance of the work.

Unlike previous GIS-AHP studies on flood susceptibility, this research introduces a dual-weighting validation framework that enhances both the credibility and applicability of the results. While most existing studies rely on a single source of weighting, typically based on either literature or expert judgment, this study integrates two independent AHP models: one constructed using weights derived from established literature, and another developed through a structured expert-based questionnaire targeting professionals in hydrology and flood risk management.

Several recent studies have applied GIS-based multi-criteria decision-making (MCDM) approaches, including AHP and fuzzy-AHP, for flood susceptibility mapping in arid and semi-arid environments. For instance, Elsheitk et al. (2024) demonstrated the usefulness of integrating GIS with hydrological simulations, while Elsaid et al. (2023) employed morphometric and statistical indices to delineate flood-prone zones. These works provided

valuable insights; however, they typically relied on single-weighting AHP frameworks or required extensive hydrological data that is often unavailable in data-scarce basins. Moreover, while some studies have highlighted susceptibility mapping, few have directly connected their results to practical flood mitigation measures, such as dam site selection and rainfall harvesting.

In contrast, the present study introduces a novel dual-weighting strategy that combines two independent AHP applications: one derived from literature-based weights and another based on expert judgment collected through a structured survey. This approach enabled a robust internal validation, with the two resulting maps showing a very high spatial agreement of 98% and a Kappa coefficient of 0.995, thus ensuring methodological consistency and credibility. External validation was also performed by comparing the susceptibility outputs with historical flood records from satellite imagery, confirming their reliability despite the limited hydrological data available in the study area. Most importantly, this research goes beyond mapping susceptibility by explicitly linking GIS-AHP outputs with hydrological modeling tools (SCS-CN and HEC-HMS) to estimate runoff volumes and to identify optimal storage dam sites for rainfall harvesting.

Accordingly, while existing works have made significant contributions, they remain constrained by methodological limitations, a lack of rigorous validation, or limited applicability to flood mitigation planning. The integrated framework developed here, combining GIS, dual AHP weighting, and hydrological modeling, offers a scientifically rigorous and practically relevant advancement that strengthens both the novelty and applicability of flood susceptibility studies in arid regions such as Wadi Ked.

The resulting flood susceptibility maps were compared using spatial overlay analysis in ArcGIS. The validation process revealed a high spatial agreement of 98% and a Cohen's Kappa coefficient of 0.995, indicating near-perfect consistency between the two outputs. This novel comparative approach addresses the limitations of single-source AHP applications by demonstrating the robustness, transferability, and flexibility of the model under different knowledge inputs.

To the best of our knowledge, this is the first flood susceptibility study in Wadi Ked by:

- Apply an integrated GIS-AHP framework for spatial flood risk assessment.
- Link flood hazard mapping directly with dam site identification for water harvesting; and
- Validate AHP-derived maps using a dual-source comparison supported by statistical agreement metrics.

To further highlight the contribution of this study, a comparative review of recent GIS-MCDM flood susceptibility studies is presented in Table 1, which provides a structured comparison between recent high-quality studies on flood susceptibility mapping and the current work. While earlier studies have applied AHP, fuzzy-AHP, or morphometric indices with varying levels of validation, most lacked dual weighting strategies, comprehensive validation metrics, or a direct linkage to dam site selection. The present study addresses these gaps by

TABLE 1 | Comparative analysis of recent GIS–MCDM flood susceptibility studies (2021–2024) and the novelty of the present study.

Recent Study	Method	Validation	Limitation	How this study is different
Alarifi et al. (2022) (SW Saudi Arabia)	GIS + AHP	Consistency ratio (CR) only	Single weighting scheme; limited link to flood mitigation	Our study applies dual AHP weighting (literature vs. expert) and integrates with the dam site identification
Elsadek and Almaliki (2024) (KSA, Al-Sail Al-Kabir basin)	Morphometric + hydrological indices + AHP	Basic consistency checks only	Focused on susceptibility mapping only; no direct validation with expert-based weights	Our study introduces comparative dual validation (98% agreement, Kappa = 0.995), ensuring robustness
Lahmer et al. (2023) (North Africa)	GIS + fuzzy-AHP	AUC-ROC analysis only	Strong at statistical validation but weak at linking results to practical flood mitigation	Our study goes beyond statistical metrics by linking susceptibility maps to hydrological modeling outputs (HEC-HMS, SCS-CN) for dam siting
This Study (Wadi Ked, Egypt)	GIS + Dual AHP (literature and expert) + HEC-HMS + SCS-CN	Spatial overlay (98% agreement) + Kappa (0.995)	Limited observed hydrological event data (acknowledged in limitations)	First study in Wadi Ked to combine dual validation of AHP with hydrological modeling for actionable dam sitting and rainfall harvesting in an arid catchment

integrating dual AHP weighting (literature- and expert-based), quantitative validation (spatial agreement and Kappa coefficient), and hydrological modeling as HEC-HMS (Hydrologic Engineering Center–Hydrologic Modeling System and Soil Conservation Service Curve Number [SCS-CN]), thereby positioning itself as a novel contribution to flood risk assessment in arid catchments.

This methodological advancement provides a replicable and cost-effective decision-support tool for flood-prone, data-scarce arid regions, and fills a key gap in the regional literature on flood hazard management.

2 | Materials and Methods

2.1 | Study Area

The Sinai Peninsula spans both North Africa and Southwest Asia, serving as a transitional area between the climates of the northern Mediterranean and the Sahara (EEAA 2005). This research centers on Wadi Ked in South Sinai, Egypt, positioned between 34°5'E and 34°25'E longitude and 28° 5'N and 28°30'N latitude. It covers an area of approximately 1056 km² with a perimeter of about 211 km. The highest and lowest elevations are 2421 m and 0 m above mean sea level (a.m.s.l.), respectively. Wadi Ked drains into the Gulf of Suez, as illustrated in Figure 1.

2.2 | Methods

MCDM and AHP were utilized to pinpoint and map areas in the study region that are susceptible to flooding. The spatial

data layers of the 11 factors influencing flood occurrence (E), (S), (R), (DS), (DR), (DD), (TWI), (LULC), (NDVI), (ST), and (C) were prepared in raster format. These layers were created using GIS and remote sensing techniques, utilizing data from various sources, as shown in Figure 2.

All raster factor maps were standardized to a uniform measurement scale, ranging from 1 (very low) to 5 (very high), using ArcGIS. Subsequently, the maps were then rescaled to a resolution of 10 m. After reclassifying all factor maps that affect the flash flood, the (AHP) framework was applied to provide an estimated effect weight to each factor. The area's flood susceptibility map has been generated using (11) flooding-related components in ArcGIS using the weighted overlay approach.

In this study, hydrological simulations were performed using the Hydrologic Engineering Center–Hydrologic Modeling System (HEC-HMS), a widely applied rainfall–runoff model developed by the U.S. Army Corps of Engineers. The model estimates flood hydrographs based on rainfall input, watershed characteristics, and runoff generation methods. Runoff was computed using the Soil Conservation Service–Curve Number (SCS-CN) method, which relates land use/land cover, hydrologic soil group, and antecedent moisture conditions to rainfall–runoff conversion. Key outputs from HEC-HMS include direct runoff depth, peak discharge (Q_p), and lag time (t_L), which were used to evaluate the hydrological feasibility of proposed dam sites.

2.3 | Data Types and Sources

The Sinai Peninsula experiences an arid or semi-arid climate. The average temperatures in the month range from

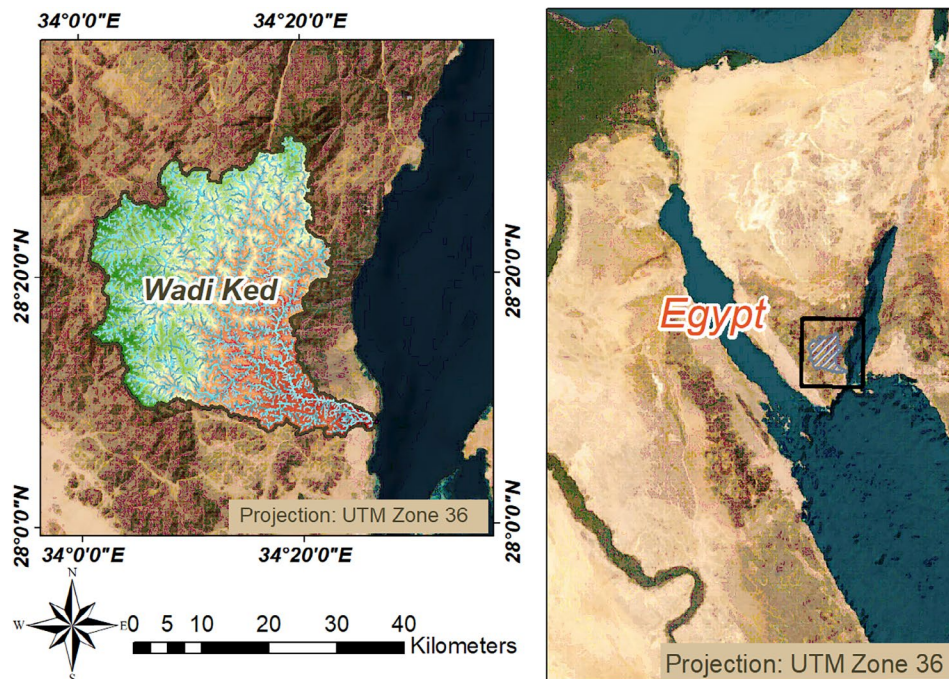


FIGURE 1 | Location of Wadi Ked.

approximately 14°C–40°C, respectively, from January to August. Meanwhile, the average relative humidity varies from 25% to 44%. Precipitation levels are typically low and decline from the northeastern to the southwestern areas. The highest annual rainfall, reaching 304 mm, was recorded by the Rafah station in the northeast (Hegazi and Bagouri 2011). Most of the precipitation occurs during winter, with a monthly average ranging from zero in July to 6.7 mm in January (Ahmed and Diab 2018). Therefore, the Sinai Peninsula is an extremely arid environment, with the rate of evaporation significantly surpassing the rate of precipitation (Hermas et al. 2012).

The data necessary for this study were gathered from various sources, as shown in Table A1. A Digital Elevation Model (DEM) with a 30-m spatial resolution was obtained from the U.S. Geological Survey (USGS) website to retrieve various flood-controlling factors.

The USGS website provided 10-m resolution imagery from satellites obtained on January 27, 2022. The NDVI factor map was generated using the satellite image's red bands. The Sentinel-2A image collection date was intentionally chosen to decrease climatic interference, coinciding with the arid season, during which monthly cloud cover is either minimal or nonexistent. A precise and high-resolution Sentinel-2 (LULC) map for 2023, with a resolution of 10 m, was obtained from the Environmental System Research Institute (ESRI) website.

The Thiessen polygons demonstrate that the Sant Catherine, Dahab, and Sharm Sheikh stations exclusively impact the study area, as depicted in Figure 3a. Precipitation data for these stations were gathered from the Water Resources Research Institute (WRRI) and are indicated in Figure 3b.

2.4 | Preparing and Reclassifying the Flood-Controlling Factors Maps Approaches

In flood susceptibility mapping using GIS, the factors to consider are not fixed, and no standard guidelines exist for selecting them. In this study, 11 factors related to flood occurrence were chosen after considering previous research, data accessibility, expert insights, and the physical characteristics of the study area.

The next section outlines the factors included in this study and the techniques applied to process and prepare each factor map. The DEM was obtained at a 30-m resolution from the website of the USGS (USGS United States Geological Survey 2020). The DEM was obtained using the Geographic Coordinate Systems—World Geodetic System (GCS-WGS 1984) projection. Before loading the data into GIS software, it was aligned with the WGS 1984—Universal Transverse Mercator (UTM)—Zone 36 coordinate system. Following this, the Wadi Ked area was extracted from the DEM and readied for hydrological, topographic, and morphometric analysis, with elevation levels ranging from 0 to 2421 m.

The study area's DEM, which represents a continuous surface where each cell denotes the elevation of a specific location, has been classified into five flood susceptibility categories. Additionally, it has been adjusted to generate an elevation factor map. The slope of the land refers to the angle of the Earth's surface within the basin relative to the horizontal plane (Meshram and Khadse 2015). This outcome is influenced by several important factors, including the climate and the type of rock present within the basin (Dhawaskar 2015). It plays a crucial role in hastening surface runoff (Lalbiakmawia 2015). As the slope increases, the outflow becomes more pronounced (Shultz 2007).

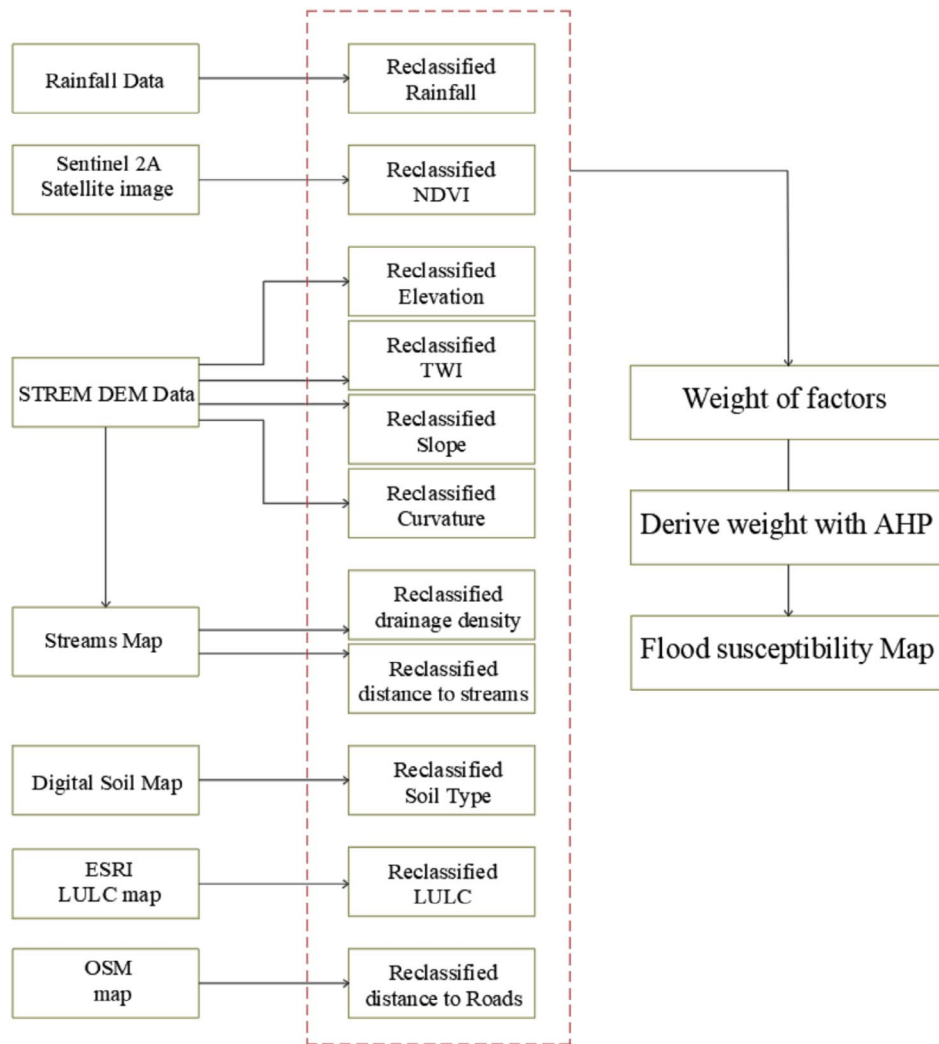


FIGURE 2 | Flowchart detailing the methods employed to identify and map areas prone to flooding.

The gradient and deformation maps were generated from the research area's DEM using ArcGIS's slope and curvature features. In much of southern Sinai, rainfall is generally scarce, sporadic, and influenced by fluctuations in the climate. The area is known for its irregular and unpredictable precipitation, coupled with consistently high temperatures throughout the year. Rainfall primarily occurs during the spring and autumn seasons (Ibrahim 2004).

The Thiessen polygons demonstrate that the Sant Catherine, Dahab, and Sharm el-Sheikh stations exclusively impact the study area, as depicted in Figure 3. Precipitation data for these stations were gathered from the WRRI to prepare the rainfall factor map. Subsequently, the mean annual rainfall from the three stations was interpolated using the Inverse Distance Weighted (IDW) method in the ArcGIS 10.3 environment. The resulting data was then trimmed using the boundary shapefile of Wadi Ked to generate a seamless rainfall map for the area. The drainage density is the ratio of the total length of streams within an area to the area's size (Zzaman et al. 2021). As drainage density increases, so does surface runoff and the likelihood of flooding (Abdelkarim et al. 2020; Das and Gupta 2021). The streams map for Wadi Ked was derived from the DEM utilizing ArcGIS. Subsequently, the drainage density map was obtained

using the tools of the ArcGIS 10.3 program, which was derived from the previously generated streams map. The distance to the streams raster map was generated using the Euclidean Distance tool in the ArcGIS environment, based on the streams map of Wadi Ked.

The (TWI) map of the area was generated using (Equation 1) proposed by (Moore et al. 1991). The TWI map of wadi Ked was obtained using the Raster Calculator tool in the ArcGIS environment's Spatial Analyst Tools.

$$TWI = \ln \left(\frac{A_s}{\tan B} \right) \quad (1)$$

In this equation, A_s denotes the entire upslope area flowing via a particular location (per unit contour length), and B represents the regional gradient angle in degrees. To create the LULC factor map, a LULC map for the study area was initially extracted from an LULC map obtained from the ESRI website. Since integers originally represented the classes in the obtained LULC map, each class was then assigned the proper descriptions using ArcGIS software. The scrub/shrub area and bare ground together constitute almost the entire surface area of Wadi Ked.

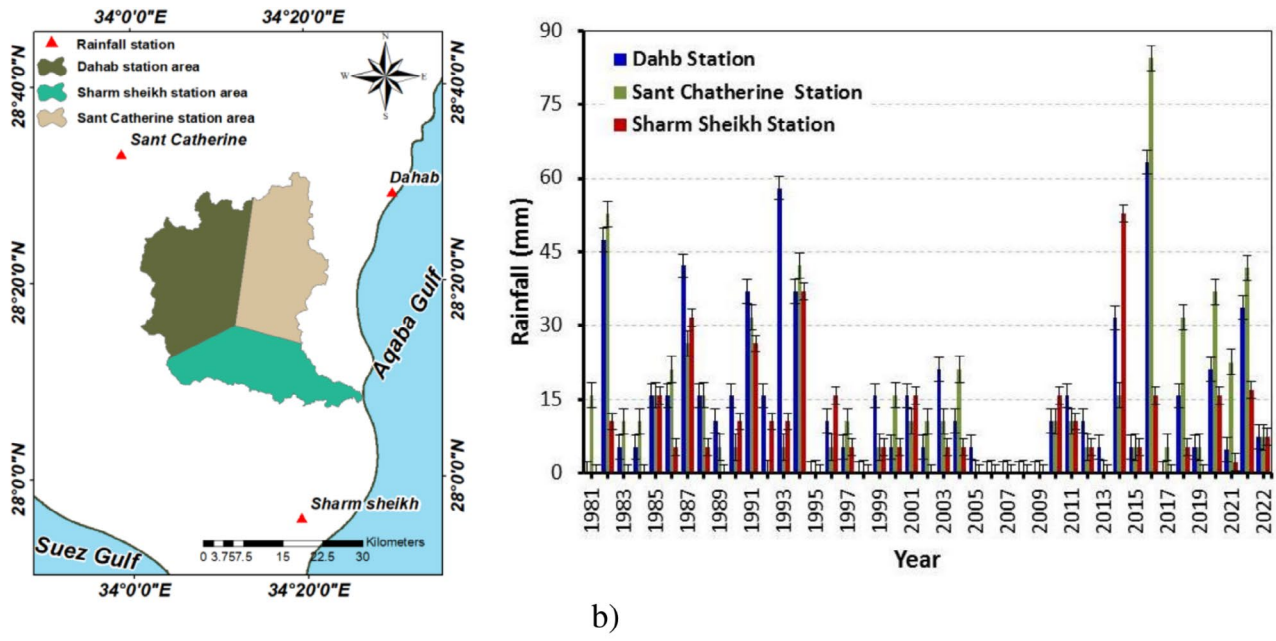


FIGURE 3 | Wadi Ked for (a) Thiessen polygons for the rainfall station's location and (b) rainfall data from the case study's rainfall stations.

Wadi Ked's soil type was first determined by employing the ArcGIS 10.3 application to extract data from the World Digital Soil Map, which was downloaded from the Food and Agriculture Organization of the United Nations (FAO) website. Satellite data from the United States (U.S.) Geological Survey website was used to construct the region's NDVI map. The NDVI map of Wadi Ked was generated from the Sentinel 2A satellite image by utilizing Equation (2) provided below.

$$NDVI = \frac{NIR - RED}{NIR + RED} = \frac{\text{Band 8} - \text{Band 4}}{\text{Band 8} + \text{Band 4}} \quad (2)$$

Curvature describes the shape of the surface topography in a specific area (Das and Gupta 2021). It represents the rate at which the slope changes in a particular direction. (Zzaman et al. 2021). The curvature map for Wadi Ked was produced directly from the DEM of the study area using curvature tools within the ArcGIS environment. The chosen factors influencing flood severity in the study region were prepared and arranged. Then they were classed into five levels, with one denoting that the area is very weakly impacted by floods and five denoting that the area is very significantly affected by floods. The factors were then rescaled to the exact spatial resolution. The classification for all characteristics was determined by evaluating previous research and the specific circumstances of the study area because there was no standardized scale for reclassifying these elements.

2.5 | Analytical Hierarchy Process

The analytical hierarchy process (AHP) method, as proposed by W. A. Saaty (1987), is widely recognized as the most used and effective technique in MCDM for determining the relative importance of each criterion or factor under consideration in a study, and numerous prior research works (Abdelkarim et al. 2020; Ajibade et al. 2021; Das and Gupta 2021;

Karymbalis et al. 2021) have used it to assign weights to each flood-controlling factor and ultimately to identify and map areas prone to flooding. The factors used for flood susceptibility mapping through MCDM were weighted based on the local physical properties of the study area and an analysis of past research.

The selection of experts for the AHP pairwise comparison questionnaire was based on clearly defined inclusion criteria to ensure the credibility and relevance of the input. Experts were purposefully selected from among professionals and academics with demonstrated experience in hydrology, water resources engineering, GIS applications, and flood risk management. Selection criteria included:

- A minimum of 5 years of relevant professional or academic experience.
- Possession of at least a master's or (Doctor of Philosophy) PhD degree in a related discipline.
- Prior involvement in flood modeling, watershed planning, or hydrological assessment projects.

The questionnaire was distributed to 40 qualified experts, including university faculty members, governmental engineers, and practitioners from national research institutes and water-related agencies, particularly the Ministry of Water Resources and Irrigation in Egypt. Responses were reviewed for completeness and consistency before being aggregated into a collective pairwise comparison matrix. This expert pool provided a diverse yet technically robust basis for assigning weights in the AHP.

In the development of the flood susceptibility model, special attention was given to the potential interaction and conflict between input factors. Specific criteria, such as elevation and rainfall, may exert opposing or context-dependent influences. To resolve such disputes, the AHP methodology was employed

to derive context-specific weights based on structured pairwise comparisons.

For instance, while high elevation often implies a lower likelihood of flooding, in Wadi Ked, elevated zones are frequently associated with steep slopes that generate rapid surface runoff. Conversely, low-lying areas may accumulate flow but not necessarily pose a higher flood risk if infiltration is adequate. Similarly, rainfall contributes significantly to flood generation, particularly when combined with compact soils or sparse vegetation.

Regional studies inform both theoretical hydrological behavior and expert judgment. As a result, the weighted overlay did not simply combine the factors arithmetically but rather integrated them through a calibrated structure that accounts for their contextual relevance and interdependence.

The following detailed processes were performed to ascertain the relative weights of each flood-controlling element utilized in this study, following W. A. Saaty's (1987) guidelines.

Each factor was assigned a value between 1 and 9 based on its relative importance to construct two separate matrices. Two matrices were developed: (Table 2) a literature-based matrix derived from previous peer-reviewed studies, and (Table 3) an expert-based matrix built from responses to a structured questionnaire distributed to hydrology and flood risk specialists. In this scale, 1 indicates equal importance, while 9 indicates extreme importance, as shown in Table A2.

After that, each value in the column of the pairwise comparison matrix was divided by the sum of its values to create the normalized pairwise comparison matrix tables (Tables 4 and 5). In the third step, the weight of all variables was determined (Tables 4 and 5) by dividing the total number of factors (in this case, 11) by the sum of each row in the normalized pairwise comparison matrix.

After the weights for each flood-controlling component have been calculated, the following equations were used to examine the accuracy and consistency of the comparisons. The consistency index (CI) was determined using Equation (3) as provided by W. A. Saaty (1987).

$$CI = \frac{\lambda_{\max} - n}{n - 1} \quad (3)$$

In the equation, CI represents the consistency index, “ n ” denotes the number of matrix elements being evaluated, and λ_{\max} is the greatest eigenvalue of the pairwise comparison matrix.

Following W. A. Saaty (1987), (λ_{\max}) was determined (Tables 6 and 7) using the following steps:

- Figuring out the product of every column's value (in the non-normalized matrix table) by the weight of the criteria.
- Adding up the data in the rows to determine the weighted sum.
- Calculating the proportion between each weighted sum value and the weight assigned to it by the criterion, and
- Calculating the mean ratios of the weighted aggregate value to the criteria weight.

Ultimately, the consistency ratio (CR) was calculated using the following equation (Equation 4), recommended by W. A. Saaty (1987), to confirm the consistency of the comparison.

$$CR = \frac{CI}{RI} \quad (4)$$

which varies based on the number of factors used in the pairwise comparison matrix as shown in Table A3. When the CR is less than 0.10, it indicates that the pairwise comparison matrix is reasonably consistent. Suppose the CR is greater than or equal to 0.10. In that case, it suggests that the pairwise comparison lacks

TABLE 2 | Matrix for pairwise comparison (this study).

Factor	E	S	R	DS	DR	DD	TWI	LULC	NDVI	C	ST
E	1.00	2.00	2.00	2.00	2.00	3.00	3.00	2.00	4.00	4.00	3.00
S	1/2	1.00	3.00	2.00	2.00	3.00	3.00	1.00	5.00	5.00	4.00
R	1/2	1/3	1.00	2.00	2.00	2.00	3.00	2.00	4.00	5.00	4.00
DS	1/2	1/2	1/2	1.00	1.00	2.00	3.00	3.00	4.00	4.00	4.00
DR	1/2	1/2	1/2	1.00	1.00	2.00	3.00	3.00	4.00	4.00	4.00
DD	1/3	1/3	1/2	1/2	1/2	1.00	2.00	2.00	4.00	5.00	3.00
TWI	1/3	1/3	1/3	1/3	1/3	1/2	1.00	1.00	3.00	4.00	2.00
LULC	1/2	1.00	1/2	1/3	1/3	1/2	1.00	1.00	3.00	4.00	2.00
NDVI	1/4	1/5	1/4	1/4	1/4	1/4	1/3	1/3	1.00	2.00	1/2
C	1/4	1/5	1/5	1/4	1/4	1/5	1/4	1/4	1/2	1.00	1/3
ST	1/3	1/4	1/4	1/4	1/4	1/3	1/2	1/2	2.00	3.00	1.00
Sum	5.00	6.65	9.03	9.92	9.92	14.78	20.08	16.08	34.50	41.00	27.83

Note: The Gray-shaded cells point to diagonal and reciprocal values in the AHP pairwise comparison matrix for clarity.

TABLE 3 | Matrix for pairwise comparison (Questionnaire).

Factor	E	S	R	DS	DR	DD	TWI	LULC	NDVI	C	ST
E	1.00	3.00	2.00	3.00	2.00	2.00	3.00	2.00	4.00	4.00	4.00
S	1/3	1.00	5.00	2.00	2.00	3.00	3.00	1.00	5.00	5.00	4.00
R	1/2	1/5	1.00	2.00	2.00	2.00	3.00	2.00	4.00	5.00	4.00
DS	1/3	1/2	1/2	1.00	1.00	2.00	3.00	3.00	4.00	4.00	4.00
DR	1/2	1/2	1/2	1.00	1.00	2.00	3.00	3.00	4.00	4.00	4.00
DD	1/2	1/3	1/2	1/2	1/2	1.00	2.00	2.00	4.00	5.00	3.00
TWI	1/3	1/3	1/3	1/3	1/3	1/2	1.00	1.00	3.00	4.00	2.00
LULC	1/2	1.00	1/2	1/3	1/3	1/2	1.00	1.00	3.00	4.00	2.00
NDVI	1/4	1/5	1/4	1/4	1/4	1/4	1/3	1/3	1.00	2.00	1/2
C	1/4	1/5	1/5	1/4	1/4	1/5	1/4	1/4	1/2	1.00	1/3
ST	1/4	1/4	1/4	1/4	1/4	1/3	1/2	1/2	2.00	3.00	1.00
Sum	4.75	7.52	11.03	10.92	9.92	13.78	20.08	16.08	34.50	41.00	28.83

Note: The Gray-shaded cells point to diagonal and reciprocal values in the AHP pairwise comparison matrix for clarity.

TABLE 4 | Matrix showing the normalized pairwise comparison (this study).

Factor	E	S	R	DS	DR	DD	TWI	LULC	NDVI	C	ST	Factor weight
E	0.20	0.30	0.22	0.20	0.20	0.20	0.15	0.12	0.12	0.10	0.11	17%
S	0.10	0.15	0.33	0.20	0.20	0.20	0.15	0.06	0.14	0.12	0.14	16%
R	0.10	0.05	0.11	0.20	0.20	0.14	0.15	0.12	0.12	0.12	0.14	13%
DS	0.10	0.08	0.06	0.10	0.10	0.14	0.15	0.19	0.12	0.10	0.14	12%
DR	0.10	0.08	0.06	0.10	0.10	0.14	0.15	0.19	0.12	0.10	0.14	12%
DD	0.07	0.05	0.06	0.05	0.05	0.07	0.10	0.12	0.12	0.12	0.11	8%
TWI	0.07	0.05	0.04	0.03	0.03	0.03	0.05	0.06	0.09	0.10	0.07	6%
LULC	0.10	0.15	0.06	0.03	0.03	0.03	0.05	0.06	0.09	0.10	0.07	7%
NDVI	0.05	0.03	0.03	0.03	0.03	0.02	0.02	0.02	0.03	0.05	0.02	3%
C	0.05	0.03	0.02	0.03	0.03	0.01	0.01	0.02	0.01	0.02	0.01	2%
ST	0.07	0.04	0.03	0.03	0.03	0.02	0.02	0.03	0.06	0.07	0.04	4%

adequate consistency, and the comparison process should be repeated until the CR value falls below 0.10 (W. A. Saaty 1987).

2.6 | Flood Susceptibility Map Preparation Method

The spatial layers were combined and superimposed in the ArcGIS environment's Spatial Analyst Extension after each flood-controlling factor was prepared, reclassified using ArcGIS software to a common scale, and weighted using the AHP approach. This was done using the weighted overlay technique, which applies equation (Equation 5) given below to derive the flood susceptibility map of the study area. Several prior studies (Ali et al. 2020; Allafta and Opp 2021; Aydin and Birincioğlu 2022) have utilized Equation (5) to produce the flood vulnerability map.

$$FS = \sum_{i=0}^n x_i \times w_i \quad (5)$$

In the equation, FS represents Vulnerability to Flooding; n stands for the number of decision criteria. x_i denotes the specific standardized criterion, and w_i is the corresponding weight of the criterion. The cell or pixel values of the raster layers are scaled by their corresponding weights or percentage influences derived from the AHP analysis. The resulting values are then summed to generate the flood susceptibility output raster map.

3 | Results and Discussion

3.1 | Processing of Flood-Controlling Factors

The study mapped and identified positions vulnerable to flood inundation using eleven flood-controlling parameters. The research area's spatial distribution of flood susceptibility was determined and mapped by examining and analyzing these factors. The analysis for each element is described in more detail below.

TABLE 5 | Matrix showing the normalized pairwise comparison (Questionnaire).

Factor	<i>E</i>	<i>S</i>	<i>R</i>	<i>DS</i>	<i>DR</i>	<i>DD</i>	<i>TWI</i>	<i>LULC</i>	<i>NDVI</i>	<i>C</i>	<i>ST</i>	Factor weight
E	0.21	0.40	0.18	0.27	0.20	0.15	0.15	0.12	0.12	0.10	0.14	18%
S	0.07	0.13	0.45	0.18	0.20	0.22	0.15	0.06	0.14	0.12	0.14	17%
R	0.11	0.03	0.09	0.18	0.20	0.15	0.15	0.12	0.12	0.12	0.14	13%
DS	0.07	0.07	0.05	0.09	0.10	0.15	0.15	0.19	0.12	0.10	0.14	11%
DR	0.11	0.07	0.05	0.09	0.10	0.15	0.15	0.19	0.12	0.10	0.14	11%
DD	0.11	0.04	0.05	0.05	0.05	0.07	0.10	0.12	0.12	0.12	0.10	8%
TWI	0.07	0.04	0.03	0.03	0.03	0.04	0.05	0.06	0.09	0.10	0.07	6%
LULC	0.11	0.13	0.05	0.03	0.03	0.04	0.05	0.06	0.09	0.10	0.07	7%
NDVI	0.05	0.03	0.02	0.02	0.03	0.02	0.02	0.02	0.03	0.05	0.02	3%
C	0.05	0.03	0.02	0.02	0.03	0.01	0.01	0.02	0.01	0.02	0.01	2%
ST	0.05	0.03	0.02	0.02	0.03	0.02	0.02	0.03	0.06	0.07	0.03	4%

TABLE 6 | Evaluating the consistency of pairwise comparisons (CR=0.052) (this study).

Factor	<i>E</i>	<i>S</i>	<i>R</i>	<i>DS</i>	<i>DR</i>	<i>DD</i>	<i>TWI</i>	<i>LULC</i>	<i>NDVI</i>	<i>C</i>	<i>ST</i>	WSV weighted sum value	FW (factor weight)	WSV/FW
E	0.17	0.32	0.26	0.24	0.24	0.24	0.18	0.14	0.12	0.08	0.12	2.11	0.17	12.07
S	0.09	0.16	0.39	0.24	0.24	0.24	0.18	0.07	0.15	0.10	0.16	2.02	0.16	12.24
R	0.09	0.05	0.13	0.24	0.24	0.16	0.18	0.14	0.12	0.10	0.16	1.61	0.13	12.16
DS	0.09	0.08	0.07	0.12	0.12	0.16	0.18	0.21	0.12	0.08	0.16	1.38	0.11	12.04
DR	0.09	0.08	0.07	0.12	0.12	0.16	0.18	0.21	0.12	0.08	0.16	1.38	0.11	12.04
DD	0.06	0.05	0.07	0.06	0.06	0.08	0.12	0.14	0.12	0.10	0.12	0.98	0.08	11.78
TWI	0.06	0.05	0.04	0.04	0.04	0.04	0.06	0.07	0.09	0.08	0.08	0.65	0.06	11.53
LULC	0.09	0.16	0.07	0.04	0.04	0.04	0.06	0.07	0.09	0.08	0.08	0.81	0.07	11.50
NDVI	0.04	0.03	0.03	0.03	0.03	0.02	0.02	0.02	0.03	0.04	0.02	0.32	0.03	11.44
C	0.04	0.03	0.03	0.03	0.03	0.02	0.02	0.02	0.02	0.02	0.01	0.26	0.02	11.55
ST	0.06	0.04	0.03	0.03	0.03	0.03	0.03	0.04	0.06	0.06	0.04	0.44	0.04	11.33

$$\lambda_{\max} = 11.79$$

3.2 | Land Use Land Cover

Land use land cover (LULC) are a crucial factor in flood occurrence. Due to its ability to slow down the rapid flow of water and promote high levels of infiltration, areas with dense vegetation are often less prone to flood risk. In urban and residential areas, runoff tends to increase due to impermeable surfaces and limited infiltration (Das and Gupta 2021). Allafta and Opp (2021) categorized shrub land, cropland, bare land, urban areas, and waterbodies as having very low, low, moderate, high, and very high susceptibility to flooding, respectively. In this study, the LULC map of the study area (Figure A1) is classified into three categories: very high susceptibility to floods (water bodies), high susceptibility (bare land), and low susceptibility (shrub/shrub land). The primary LULC

type in Wadi Ked is bare land, which constitutes around 87% of the study area. Tables A4 and A5 indicate a high susceptibility to flooding. Shrub/shrubland covers approximately 13%. Although “bare land” may seem hydrologically neutral in conventional land cover analyses, its behaviour in arid and semi-arid environments, such as Wadi Ked, significantly increases flood susceptibility. In this study, bare land covers approximately 87% of the total area. These surfaces are typically characterized by compacted soils, a crusted top layer, and a complete lack of vegetation, all of which drastically reduce infiltration capacity. Under arid climatic conditions, rainfall is often of high intensity and short duration, leading to rapid conversion of precipitation into surface runoff. The absence of vegetation limits interception, while crusted surfaces promote overland flow, resulting in enhanced flash flood

TABLE 7 | Evaluating the consistency of pairwise comparisons (CR=0.0657) (Questionnaire).

Factor	E	S	R	DS	DR	DD	TWI	LULC	NDVI	C	ST	WSV weighted sum value	FW (Factor weight)	WSV/ FW
E	0.18	0.51	0.26	0.33	0.22	0.16	0.18	0.14	0.12	0.08	0.16	2.34	0.18	13.00
S	0.06	0.17	0.65	0.22	0.22	0.24	0.18	0.07	0.15	0.10	0.16	2.22	0.17	13.06
R	0.09	0.03	0.13	0.22	0.22	0.16	0.18	0.14	0.12	0.10	0.16	1.55	0.13	11.95
DS	0.06	0.09	0.07	0.11	0.11	0.16	0.18	0.21	0.12	0.08	0.16	1.34	0.11	12.18
DR	0.09	0.09	0.07	0.11	0.11	0.16	0.18	0.21	0.12	0.08	0.16	1.37	0.11	12.45
DD	0.09	0.06	0.07	0.06	0.06	0.08	0.12	0.14	0.12	0.10	0.12	1.00	0.08	12.52
TWI	0.06	0.06	0.04	0.04	0.04	0.04	0.06	0.07	0.09	0.08	0.08	0.65	0.06	10.89
LULC	0.09	0.17	0.07	0.04	0.04	0.04	0.06	0.07	0.09	0.08	0.08	0.82	0.07	11.69
NDVI	0.05	0.03	0.03	0.03	0.03	0.02	0.02	0.02	0.03	0.04	0.02	0.32	0.03	10.66
C	0.05	0.03	0.03	0.03	0.03	0.02	0.02	0.02	0.02	0.02	0.01	0.26	0.02	12.84
ST	0.05	0.04	0.03	0.03	0.03	0.03	0.03	0.04	0.06	0.06	0.04	0.43	0.04	10.67
													λ_{\max}	11.99

potential. These hydrological dynamics justify the assignment of moderate to high susceptibility levels to bare land areas in the flood risk map.

This classification is further supported by satellite imagery and field observations, which confirm the frequent occurrence of water accumulation and shallow sheet flooding across these un-vegetated, impermeable zones during past storm events.

3.3 | Elevation

Elevation (E) is a key factor in evaluating flood risk. Typically, lower-lying areas are more prone to flooding than higher elevations due to higher river discharge and faster inundation by high water flow (Hong, Panahi, et al. 2018; Lee and Rezaie 2022; Zzaman et al. 2021). The study area's altitude varies between 0 and 2421m above sea level, as depicted in Figure A1b. Approximately 16% (171.39km²) and 11% (113.01km²) of the study area are categorized as having very high and high susceptibility to flood inundation, respectively, as presented in Table A5.

3.4 | Slope

The downward slope of the terrain affects the pace of the water's surface flow. A lower slope (S) leads to slower water flow and a higher likelihood of flooding (Astutik et al. 2021; Das and Gupta 2021; Zzaman et al. 2021). Mountainous regions typically feature steeper slopes that hinder water accumulation, while low-lying or flat areas with gentle slopes are more prone to flood inundation (Wang et al. 2015). The reclassified slope map is presented in Figure A1c, which indicates that approximately 18% (188.27km²) of the study region has a slope ranging from 0° to 10°, indicating a very high susceptibility to flooding inundation.

Approximately 24% (252.49km²) and 28% (295.60km²) of the study region are prone to flooding, categorized as high (11°–20°) and moderate (21°–28°), respectively. Areas with low (29°–37°) and very low (37°–74°) flood-prone coverage account for approximately 23% and 8% of the area, respectively, as shown in Table A5.

3.5 | Normalized Difference Vegetation Index

Normalized Difference Vegetation Index (NDVI) is a measure of vegetation density in a specific area and is used as one of the factors in determining flood susceptibility (Ali et al. 2020). Increased vegetation density reduces the speed of runoff and the likelihood of flood inundation (Tehrany et al. 2017). As depicted in Figure A1, this study classified areas with NDVI values ranging from −0.264 to −0.0113, −0.0112 to 0.00856, 0.00857 to 0.0259, 0.026 to 0.0433, and 0.0434 to 0.368 as (Very High), (High), (Moderate), (Low), and (Very Low) susceptibility to flooding, respectively. In this study, an NDVI value ranging from −0.264 to −0.0113 (indicating very high susceptibility to flooding) encompasses approximately 8% of the study area. Additionally, 21%, 30%, 26%, and 15% of the study area have NDVI values falling within the ranges of (−0.0112 to 0.00856), (0.00857 to 0.0259), (0.026 to 0.0433), and (0.0434 to 0.368), respectively, as shown in Table A5.

3.6 | Rainfall

Rainfall (R) is a crucial factor to consider in flood susceptibility analysis, as floods are closely associated with precipitation. It is the most critical factor contributing to the onset of floods, as flood inundation results from a large volume of runoff caused by heavy or prolonged rainfall (Allafta and Opp 2021; Hong, Panahi, et al. 2018; Hong, Tsangaratos, et al. 2018).

The mean annual rainfall in Wadi Ked ranges from 36 to 53 mm/year, with the following classifications based on the reclassified data: 36–40 mm as very low, 41–44 mm as low, 45–47 mm as moderate, 48–49 mm as high, and 50–53 mm as very high in terms of its contribution to flooding. The rainfall map of the study area was reclassified using the classification method used by Das and Gupta (2021), as illustrated in Figure A1. Approximately 18%, 17%, 19%, 28%, and 18% of the study area were categorized as having (Very Low), (Low), (Moderate), (High), and (Very High) susceptibility to flooding, respectively (Table A5).

3.7 | Distance to Streams

Regions in proximity to streams are more likely to experience flood inundation compared to those situated farther away (Mahmoud and Gan 2018). As the distance from the stream increases, there is typically a rise in both slope and elevation (Lee and Rezaie 2022; Zzaman et al. 2021). In the study area, areas within 300 m of the stream are classified as highly susceptible to flooding, while those within 600, 900, 1200, and > 2000 m from the river are considered to have (High), (Moderate), (Low), and (Very Low) vulnerability to flooding, respectively as presented in Figure A1 and Table A5.

3.8 | Topographic Wetness Index

TWI is a measure used to quantify the impact of topography on the generation of runoff and the accumulation of flow volume at specific locations. It illustrates the tendency of water to accumulate in a particular location or flow downhill due to gravitational force (Lee and Rezaie 2022). Topographic Wetness Index (TWI) can forecast areas prone to saturated land surfaces and those with the potential to generate overland flow (Hong, Panahi, et al. 2018; Hong, Tsangaratos, et al. 2018). TWI value is directly related to flood risk; higher TWI values indicate a greater likelihood of flood inundation (Das and Gupta 2021). The TWI values in the study area were classified into five categories of flooding susceptibility: very low (2.2–5.2), low (5.2–6.9), moderate (6.9–9.4), high (9.4–13.7), and very high (13.7–24.3), covering 43%, 36%, 14%, 5%, and 1% of the study area, respectively as shown in Figure A1g; Table A5.

3.9 | Distance From Roads

The highway network of Wadi Ked was extracted from Open Street Map (OSM). In the study area, the distance from roads is classified into five categories: (0–1740 m) for very low susceptibility, (1750–4090 m) for low susceptibility, (4100–6970 m) for moderate susceptibility, (6980–10,600 m) for high susceptibility, and (10,700–17,100 m) for very high susceptibility to flooding. This study area classification is depicted Figure A1h and summarized in Table A5.

3.10 | Drainage Density

Drainage density (DD) is a measure of the total length of streams within an area relative to the size of the region (Zzaman

et al. 2021). Increased drainage density is associated with elevated surface runoff and a greater likelihood of flooding (Abdelkarim et al. 2020; Das and Gupta 2021). The drainage density values in this research are divided into five different groups: (0.162–1.93) km/km² for very low susceptibility, (1.94–3.01 km/km²) for low susceptibility, (3.02–4.12 km/km²) for moderate susceptibility, (4.13–5.39 km/km²) for high susceptibility, and (5.4–7.82 km/km²) for very high susceptibility to flooding. This classification is depicted in Figure A1 and summarized in Table A5.

3.11 | Curvature

Curvature (C) describes the shape of the surface topography of an area (Das and Gupta 2021) or it indicates the rate of change in slope along a specific direction (Zzaman et al. 2021). A positive curvature value signifies a convex surface, while a negative value indicates a concave surface. A value close to zero suggests a flat surface. In terms of flood susceptibility, flat surfaces are highly prone to flooding, followed by concave and convex surfaces (Astutik et al. 2021). As depicted in Figure 1A, the curvature of the earth's surface in this study was categorized into three classes: Concave (−31.6 to −1.31), flat (−1.3 to 0.756), and convex (0.757 to 34.4). As illustrated in Figure 4j and detailed in Table A5, approximately 11% (118.85 km²) and 67% (703.52 km²) of the study area exhibit concave and flat curvature, respectively. The remaining 22% (234.16 km²) of the area is characterized by convex curvature. While concave or flat areas are often considered low-risk zones due to their ability to retain water in humid regions, this behavior differs significantly in arid environments such as Wadi Ked. In this study, flat terrain accounts for approximately 67% of the total area and was classified as very high flood susceptibility due to several interrelated factors.

First, the compacted and crusted surface soils typical of bare land in arid regions drastically reduce infiltration rates, even in low-slope areas. Second, the region's topography and drainage pattern result in flat zones receiving significant accumulated runoff from higher surrounding areas during storm events. Third, the absence of vegetation eliminates interception and allows water to flow more freely, even across relatively gentle slopes. Finally, satellite imagery and field reports confirm the historical presence of shallow yet widespread flooding across these flat areas, reinforcing their classification as high-risk zones.

Therefore, despite their low slope, these flat areas serve as primary receivers and spreaders of overland flow and pose a significant flood hazard under arid hydrological conditions.

3.12 | Soil Type

The soil's characteristics significantly influence the infiltration process. Soil with a fine texture composition tends to reduce infiltration and increase surface runoff. Therefore, areas covered by fine-textured soil are more prone to flooding compared to regions with coarse-textured soil (Allafta and Opp 2021). According to Figure A1, the soil types of the study area are classified as low (Lithosols) and moderate (Eutric

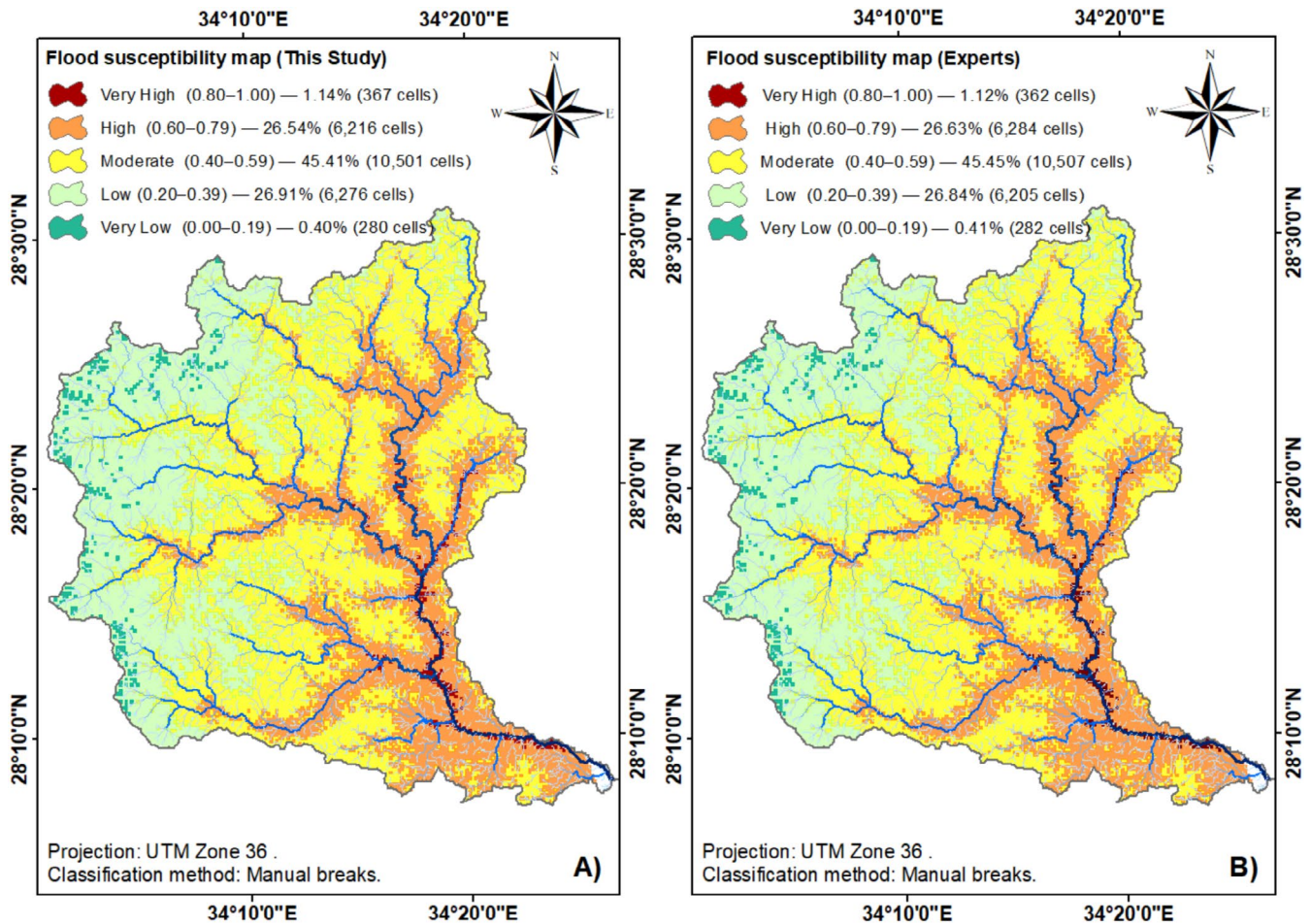


FIGURE 4 | Flood susceptibility map of Wadi Ked: (a) this study and (b) expert-based.

Regosols) susceptibility to floods. Approximately 86% of the study area is classified as having low susceptibility to flood (Table A5), while around 14% is classified as having moderate susceptibility (Table A5).

The criteria used in this study are not only supported by literature but also quantitatively justified by the physical and hydrological characteristics of Wadi Ked. For example, bare land covers 87% of the catchment with NDVI < 0.2, confirming the lack of vegetation that amplifies runoff. Similarly, 67% of the area is flat terrain prone to widespread pooling, while steep slopes > 20% in the southeast accelerate runoff and erosion. Drainage density values up to 3.1 km/km² highlight the efficiency of the channel network in concentrating flows. These site-specific conditions validate the inclusion and weighting of the 11 selected criteria in the AHP model. Table 8 summarizes the criteria together with their site-specific justification and supporting quantitative evidence, highlighting why each parameter is essential for flood susceptibility mapping in Wadi Ked.

3.13 | Analysis Using the Analytical Hierarchy Process (AHP)

For the weighted overlay method, AHP analysis was performed after each flood-controlling component was reclassified to

assign relative weights or effects on the flood-controlling variables. A pairwise comparison matrix was constructed in Tables 1 and 2, the normalization of the pairwise comparison and the calculation of the factors' weights were completed (Tables 3 and 4), and the consistency check for the comparison was conducted in Tables 5 and 6, following the procedures recommended by W. A. Saaty (1987). Table A5 displays the ultimate criteria weights for each flood-controlling factor, indicating the estimated relative impact of each factor on flooding within the study area: E (17%), S (16%), R (13%), DS (12%), DR (12%), DD (8%), TWI (6%), LULC (7%), ST (4%), NDVI (2%), and C (2%).

Among the 11 criteria used in the AHP model, elevation (17%) and slope (16%) received the highest weights due to their dominant hydrological influence on surface runoff generation in arid terrains. Elevation directly affects flow direction, drainage basin delineation, and the gravitational energy driving water movement downslope. In Wadi Ked, high-elevation zones often coincide with steeper slopes, contributing to rapid runoff accumulation in downstream areas. Slope, in turn, governs the velocity of surface flow, infiltration time, and erosional capacity. Steep slopes tend to produce faster and more concentrated runoffs, especially under intense, short-duration storms common in arid regions. These weight choices are supported by several regional studies. For example, Alarifi et al. (2022) identified elevation and slope as the most influential factors in a GIS-AHP-based

TABLE 8 | Flood-conditioning criteria and their site-specific justification in Wadi Ked.

Criterion	Site-specific justification in Wadi Ked
Elevation	Elevation ranges from ~220 to > 1500 m. The sharp relief gradient channels runoff from high mountainous upstream zones toward low-lying downstream plains, increasing flood concentration.
Slope	Flat to very gentle slopes dominate ~67% of the basin, where water accumulates and spreads widely. In contrast, slopes > 20% in the southeastern catchment accelerate runoff and generate flash flood peaks.
Rainfall	Annual rainfall averages 50–90 mm, but short-duration storms can exceed 30 mm/h, generating sudden runoff pulses.
Drainage Density (DD)	The basin exhibits a dendritic network with DD values up to 3.1 km/km ² in some sub-basins, facilitating rapid floodwater conveyance.
Distance from Streams (DS)	Settlements and cultivated lands located within 0.5–1 km of streams are directly at risk of inundation.
Distance from Roads (DR)	Roads (particularly valley-floor alignments) cross wadis and flood-prone channels, making them highly exposed to flash floods.
Soil type (ST)	Predominantly compact sandy-loam and silt soils with low infiltration rates (< 5 mm/h), which enhance overland flow during storms.
Land use/land cover (LULC)	Bare land covers ~87% of the basin, with negligible vegetation. Agricultural land and urban uses (< 10%) cluster near channels, increasing exposure.
Normalized Difference Vegetation Index (NDVI)	NDVI values are < 0.2 across most of the basin, confirming sparse vegetation and minimal interception.
Topographic Wetness Index (TWI)	High TWI values (≥ 12) identify concave zones that act as flood accumulation points; these correspond to known water pooling sites.
Curvature (C)	Positive curvature (convex slopes) dominates uplands, generating fast runoff, while concave curvatures in the floodplain promote temporary water pooling and shallow flooding.

TABLE 9 | Flood susceptibility and area coverage for both cases.

Susceptibility class	Area (km ²)	
	This study	Expert based
Very low (1)	12.51	12.60
Low (2)	280.35	277.18
Moderate (3)	469.08	469.35
High (4)	277.67	280.71
Very high (5)	16.39	16.13

flood hazard mapping study conducted in southwestern Saudi Arabia. Similarly, Elsadek and Almaliki (2024) found the same two factors to dominate flood risk assessments in the Al-Sail Al-Kabir basin, using a hydrological index-based MCDA approach.

Therefore, the prioritization of elevation and slope in this study aligns with both hydrological theory and empirical evidence from comparable dry land catchments. The calculation of the Consistency Index (CI) was based on Equation (3), and the consistency ratio (CR) was determined using Equation (4). In calculating the CI, the highest eigenvalue obtained (λ_{\max}) and the number of factors ($n = 11$) were utilized. For the CR calculation, a random index (RI) of 1.51 was employed, as shown in Table A3. The computed consistency ratio (CR), which is indicated in Table A6, falls within an acceptable range for using the comparison in weighted overlay, as it is lower than 0.1 (10%).

3.14 | Study the Area's Flood Vulnerability Map

As depicted in Figure 4a,b, the maps of 11 flood-controlling elements were integrated to form Wadi Ked's final flood-prone map. From very high (5) to very low (1) flood vulnerability, the case study was divided into five classes using the weighted overlay cooperation method. Table 9 displays the area estimates for each susceptibility class.

3.15 | Model Validation and Cross-Comparison of AHP Results

To validate the reliability and consistency of the flood susceptibility model, a spatial agreement analysis was performed between two independently generated maps. The first map was derived from AHP weights based on previous literature, while the second map utilized expert-based AHP weights obtained through a structured questionnaire.

Both maps were classified into five flood susceptibility classes (Very Low to Very High) using the same criteria layers and reclassified raster outputs as shown in Figure 4A and Figure 4B respectively. To quantify the spatial agreement, a pixel-wise comparison was carried out using the Raster Calculator tool in ArcGIS. A binary raster was created to represent matching and non-matching pixels between the two maps, as shown in

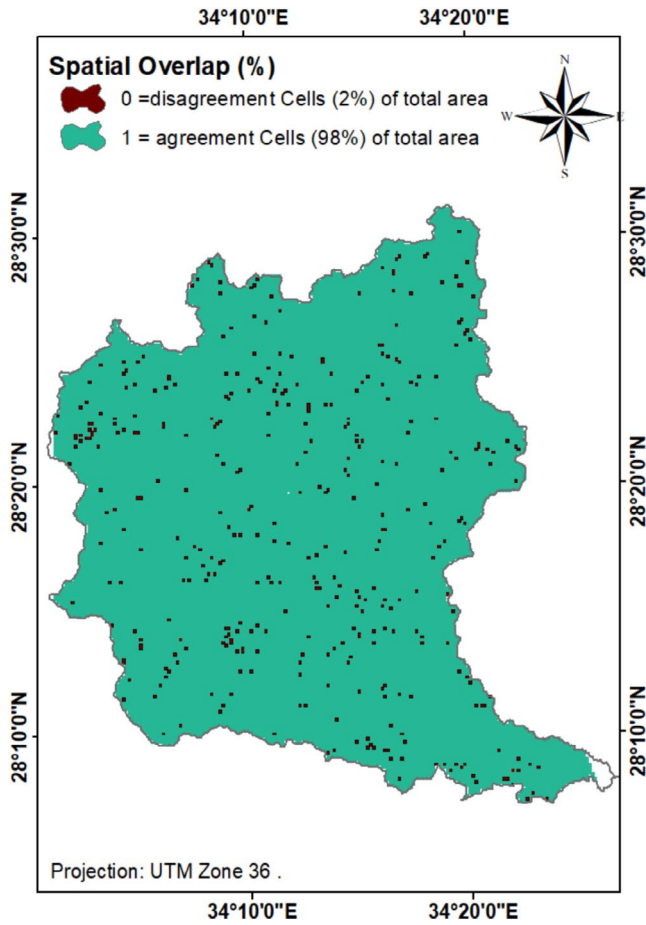


FIGURE 5 | The overall spatial agreement map of Wadi Ked (Source: Overlay of literature-based AHP and expert-based AHP).

Figure 5. This allowed the calculation of the overall spatial agreement, which was found to be 98%, indicating a high level of consistency across different weighting sources.

In addition to spatial overlay analysis, a statistical validation metric, Cohen's Kappa Coefficient (K) was employed to assess the level of agreement between the two flood susceptibility maps beyond what could occur by chance. The Kappa coefficient is a widely used index for comparing categorical classifications and is particularly appropriate when evaluating agreement between two maps derived from different sources.

To calculate the Kappa value, both maps were reclassified into five standardized susceptibility classes. A confusion matrix was constructed by cross-tabulating the number of cells in each class of both maps. The observed agreement (P_o) was computed as the proportion of matching cells (i.e., same class in both maps), which yielded a value of 0.99678. The expected agreement by chance (P_e) was calculated based on the product of the class probabilities in each map, resulting in $P_e = 0.33738$. The Kappa value was then calculated using Equation (6).

$$K = \frac{P_o - P_e}{1 - P_e} \quad (6)$$

In this study, the observed agreement was 98%, resulting in a Kappa coefficient of 0.995, as shown in (Table A7). According to

(Landis and Koch 1977) interpretation scale, this value represents “almost perfect agreement” as shown in (Table A8), thereby confirming the consistency and reliability of the model results, regardless of the weight derivation method. In the absence of sufficient hydrological observations for Wadi Ked, direct quantitative validation against gauged flood discharge data could not be undertaken. Instead, the validation of the flood susceptibility model was performed using a two-tiered approach. First, an internal cross-validation was carried out by comparing the outputs of two independently developed AHP weighting schemes (literature-based vs. expert-based), confirming a high level of model robustness. Second, an external qualitative validation was conducted by cross-checking the mapped high-risk zones with documented historical flood locations derived from satellite imagery and government reports, which showed strong consistency between predicted and observed flood-affected areas.

Nevertheless, the lack of continuous observed hydrological data in this arid catchment remains a limitation. Future research should focus on establishing systematic field monitoring networks and integrating discharge and runoff records, which would allow for more rigorous quantitative validation and further enhance the predictive reliability of flood susceptibility assessments in Wadi Ked and comparable environments.

3.16 | Runoff Estimation Using the SCS Curve Number Method

3.16.1 | The Screening of Rainfall Data

Rainfall data screening is necessary to verify outliers and ensure data homogeneity. Barnett and Lewis (1984) define an outlier as a value that is inconsistent with other values in the dataset. Hawkins (1980) describes an outlier as a record that deviates significantly from other documents, raising doubts about its accuracy. The records for the Abou Rudes station were screened for outliers using the equations from Charles, as cited in Maher et al. (2022), as follows:

$$Y_{\text{high}} = Y_{\text{ave}} + Kn \sigma_y \quad (7)$$

$$Y_{\text{low}} = Y_{\text{avg}} - Kn \sigma_y \quad (8)$$

$$K_n = 1.055 + 0.981 \log(n) \quad (9)$$

where (n) represents the number of records, (σ_y) denotes the standard deviation of the data, (Y_{high} , Y_{low}) denotes the high and the low outlier in log units, and (K_n) is the coefficient of the outlier dependent on the number of records.

The results indicated that there were no outlier readings in the collected data from the rainfall stations, as shown in Table A9.

3.17 | Runoff Estimation of Wadi Ked

Curve number (CN) is a key parameter used in the SCS-CN method to estimate surface runoff. The values of CNs range from 0 to 100 and depend on the land use and hydrologic soil group (HSG), as depicted in the land use map (Figure 6a) and

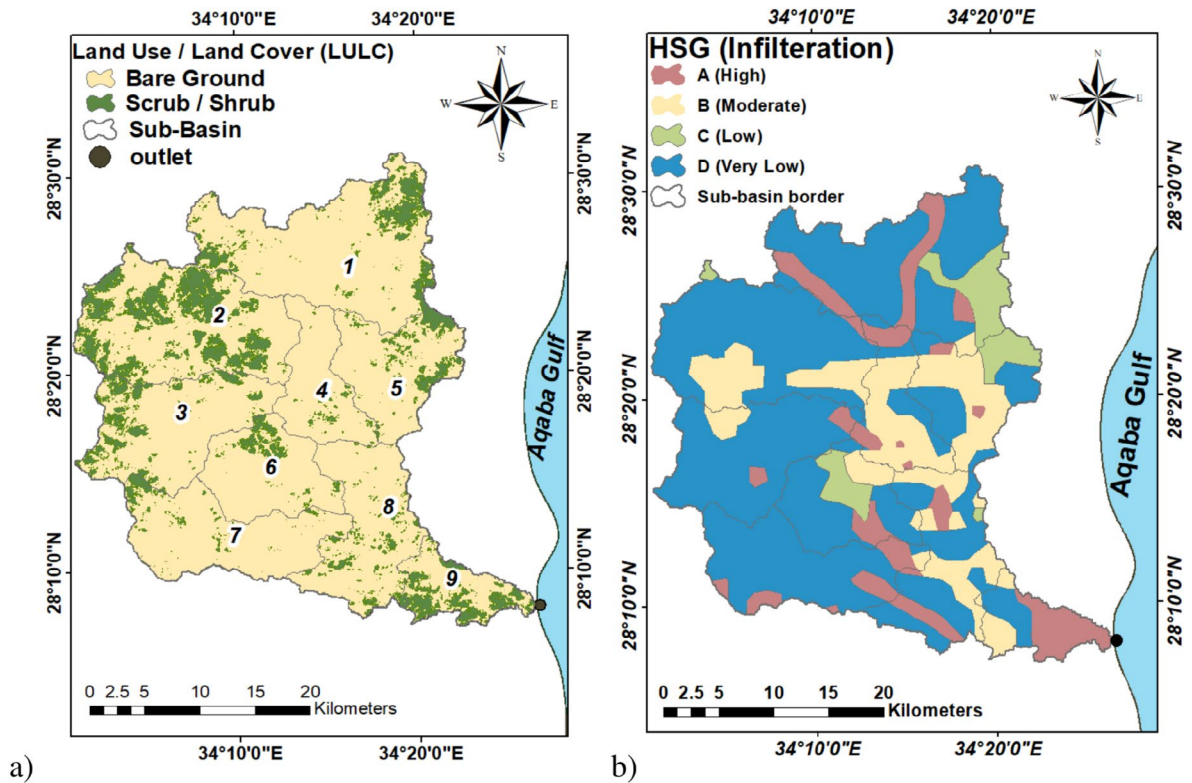


FIGURE 6 | Wadi Ked for (a) land use/land Cover and (b) values of HSGs.

HSG map (Figure 6b) of Wadi Ked. Arid and semi-arid places are the only ones with these values. To determine the curve number for each Wadi Ked sub-basin, these maps were incorporated into the ArcGIS software. The equivalent curve number (CN) for sub-basins was determined, as indicated in Table A10 (Satheeshkumar et al. 2017). The model output in this work was verified by comparing it with past flood occurrences, and there was a sufficient degree of agreement between the model-generated flood susceptibility map and the historical flood events observed in the field.

Frequency analysis is a straightforward technique used to forecast storm depth or the likelihood of its recurrence period based on historical precipitation data records. Microsoft Excel software was utilized to determine the best-fitting curve that represents the data from rainfall stations. The best-fitting curve is of the Log Pearson type III. The frequency analysis results for Wadi Ked indicate rainfall depths of 64.7mm and 75.8mm for return periods of 50 and 100 years, respectively, with a total area of 1056.60km², as displayed in Table A4.

Several computer programs are available for simulating the rainfall-runoff relationship (Al-Weshah 2002). The chosen software for simulating Wadi Ked is the Hydrologic Modeling System (HEC-HMS). This software can calculate basin parameters, such as area, slope, runoff volume, and concentration time, and conduct automated watershed delineation (Ibrahim et al. 2023). It can also function as a graphical user interface for different hydraulic and hydrologic models. Additionally, it offers various display options for presenting terrain surfaces and exporting generated images. The hydrographs for Wadi Ked, developed for the 50-year and 100-year return periods, are shown

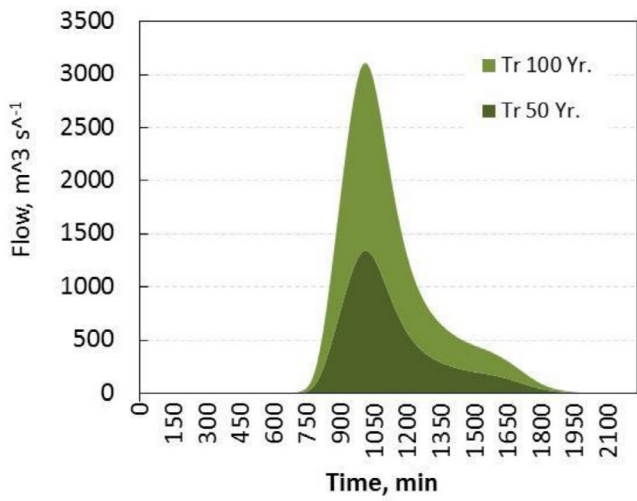


FIGURE 7 | The hydrograph of Wadi Ked for different return periods.

in Figure 7. The results extracted from the HEC-HMS Model of Wadi Ked are presented in Table A11.

3.18 | Flash Flood Protection

Floods in Egypt have resulted in significant losses, including lives, property, and infrastructure, with much of the floodwater going to waste despite its critical need (Ibrahim et al. 2023). As a result, this study aims to propose several solutions to mitigate the risks of heavy rains in Wadi Ked and to utilize

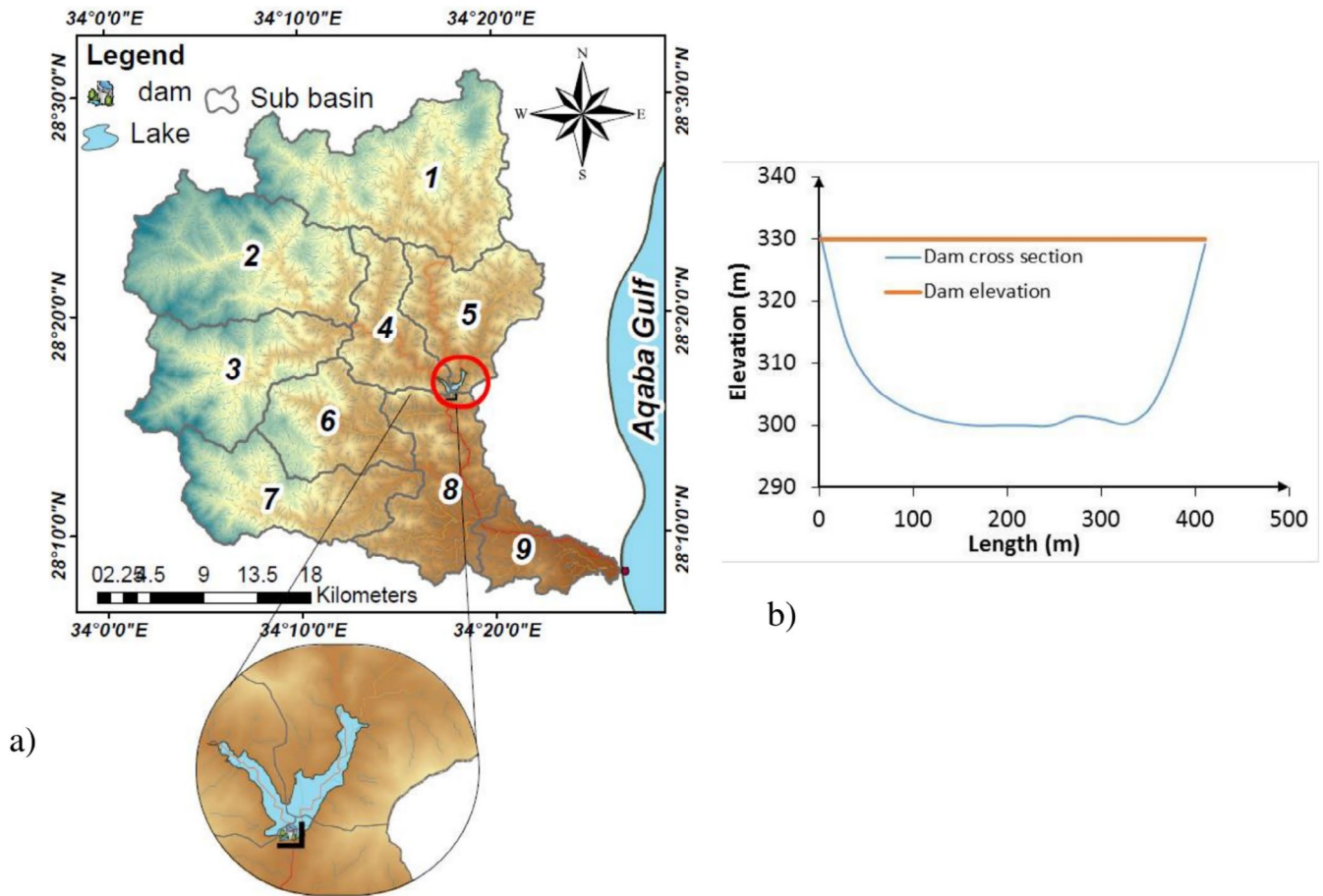


FIGURE 8 | Protection dam and Lake in wadi Ked for (a) suggested location and (b) proposed cross section.

the abundant water for various aspects of basin development. There is a scenario for the dam location in Wadi Ked. The dam's location is selected to ensure its length is suitable and constrained between two high points. It also features a lake with a storage capacity that makes it financially viable for rainfall. The proposed dam location is shown in Figure 8a. The dam specification with a lake volume is 31.74 million cubic meters (MCM), and the cross-section of the dam location is indicated in Figure 8b.

The surface runoff volumes resulting from the 50-year and 100-year storms in sub-basins No. 1 to No. 5 are 23.07 MCM and 29.66 MCM, respectively. The proposed dam's lake, with a capacity of about 31.74 MCM, is considered adequate and suitable for mitigating flood risks and utilizing the water.

4 | Conclusions

The rugged terrain and high precipitation in Wadi Ked, South Sinai, Egypt, make it highly vulnerable to flash flooding. This study integrated Geographic Information Systems (GIS) with Multi-Criteria Decision Making (MCDM) techniques, utilizing the Analytic Hierarchy Process (AHP), to identify and map flood-prone zones within the basin. Eleven flood-controlling factors, including elevation, slope, rainfall, drainage network proximity, drainage density, Topographic Wetness Index (TWI), land use/land cover, Normalized Difference Vegetation Index (NDVI), soil

type, and curvature, were analyzed, weighted, and overlaid to produce a flood susceptibility map.

The results showed that approximately 45.41% of the area falls under moderate susceptibility, while 26.54% and 1.14% are classified as high and very high susceptibility zones, respectively. Areas with low elevation, flat slopes, high drainage density, and agricultural land were most sensitive to flooding. In addition, the study identified optimal dam siting based on morphometric and hydrological analysis, with a proposed dam of 30 m in height and a storage capacity of 31.74 MCM, effectively mitigating runoff from 50- to 100-year return periods.

A key contribution of this research lies in the implementation of a dual-model AHP approach: one based on weights derived from literature and another from expert opinion collected via a structured questionnaire. The resulting susceptibility maps were compared using spatial overlay techniques and statistical validation. A high spatial agreement of 98% was observed between the two maps, and the Cohen's Kappa coefficient was calculated as 0.995, indicating "almost perfect agreement." These validation results affirm the robustness and consistency of the model.

Overall, the Geographic Information System—Analytical Hierarchy Process (GIS-AHP) framework proved to be a reliable and cost-effective tool for flood susceptibility assessment in data-scarce arid regions. The methodology and validation approach applied here can be adapted for use in other similar

catchments across arid and semi-arid zones, providing valuable support for future flood mitigation planning and water resource management.

5 | Limitations and Recommendations for Future Research

Although this study provides a structured and validated approach to flood susceptibility mapping and dam site selection using the GIS-AHP framework, several limitations must be acknowledged to guide future research and applications.

First, the Analytic Hierarchy Process (AHP), while widely adopted and transparent, inherently involves a level of subjectivity, as it relies on expert judgment for pairwise comparisons. Although this study mitigated such subjectivity by implementing a dual weighting approach (literature-based and expert-based matrices) and by ensuring consistency ratios ($CR < 0.1$), the process remains influenced by individual perspectives and expertise. Future studies may benefit from incorporating more objective weighting methods, such as entropy, fuzzy logic, or machine learning algorithms that automatically derive weights from empirical data.

Second, the study utilized static spatial layers, such as land use/land cover, NDVI, and rainfall averages, which do not reflect seasonal variability or long-term land-use changes. The flood susceptibility map generated is thus a snapshot that may need periodic updates to remain valid under changing environmental conditions. Dynamic modeling, using time-series satellite data or multi-temporal analysis, would help improve prediction accuracy and adaptability.

Third, due to the limited availability of ground-based hydrological data in Wadi Ked and the broader Sinai region, the model could not be calibrated or validated using actual discharge, flood depth, or inundation extent measurements. While spatial agreement and the Kappa coefficient were used to assess internal consistency between maps, yielding strong results (98% spatial agreement and $K = 0.995$), the absence of observed hydrological data limits the model's physical calibration. Future work should integrate field measurements or crowd-sourced flood records if available.

Fourth, the resolution of the input data, particularly the Digital Elevation Model (DEM), can impact the accuracy of runoff routing and flood risk delineation. The use of finer-resolution DEMs, LiDAR data, or high-resolution imagery may produce more detailed and locally accurate flood hazard maps, especially in narrow wadis or small sub-catchments.

Fifth, the analysis is based on a single-event flood scenario (e.g., a 50- or 100-year storm), which may not capture compound or sequential flood events. Future studies should incorporate multiple hydrological scenarios, including cumulative rainfall events, climate change projections, and soil saturation thresholds, to reflect more realistic risk conditions.

Finally, while the AHP model incorporated expert judgment from professionals in hydrology and flood management, broader

stakeholder engagement, including local planners, emergency responders, and community representatives, may provide more context-specific insights, particularly in areas where historical flood records are limited.

In conclusion, future research could enhance the robustness and applicability of GIS-based flood modeling by:

- Integrating machine learning techniques (e.g., Random Forest, SVM, or deep learning) to improve factor selection and classification accuracy.
- Coupling AHP with physically based hydrological models (e.g., HEC-HMS, SWAT, MIKE SHE) for more realistic flood simulation.
- Using time-series analysis to capture temporal variability in land cover and rainfall.
- Conducting scenario-based planning for dam siting under different land use and climate conditions.
- Expanding participatory approaches to include a broader range of stakeholders for more inclusive flood risk management.

By addressing these limitations and implementing such improvements, future studies can build upon the methodological foundation presented here to develop more robust, data-driven, and decision-supportive flood management strategies, particularly in arid and data-scarce regions like South Sinai.

Acknowledgments

The authors thank the Department of Water and Water Structures Engineering, Faculty of Engineering, Zagazig University, Zagazig 44519, Egypt, for constant support during the study.

Funding

This work was supported by Brunel University London.

Ethics Statement

The authors have nothing to report.

Consent

Informed consent was obtained from all individual participants included in the study.

Conflicts of Interest

The authors declare no conflicts of interest.

Data Availability Statement

Data sharing not applicable to this article as no datasets were generated or analysed during the current study.

References

- Abd-Elaty, I., A. Kuriqi, A. R. Ahmed, and E. M. Ramadan 2024. "Enhanced Groundwater Availability Through Rainwater Harvesting and Managed Aquifer Recharge in Arid Regions." *Applied Water Science* 14: 121. <https://doi.org/10.1007/s13201-024-02166-7>.

- Abdelkarim, A., S. S. Al-Alola, H. M. Alogayell, S. A. Mohamed, I. I. Alkadi, and I. Y. Ismail. 2020. "Integration of GIS-Based Multicriteria Decision Analysis and Analytic Hierarchy Process to Assess Flood Hazard on the Al-Shamal Train Pathway in Al-Qurayyat Region, Kingdom of Saudi Arabia." *Water* 12, no. 6: 1702. <https://doi.org/10.3390/w12061702>.
- Ahmed, A. A., and M. S. Diab. 2018. "Hydrologic Analysis of the Challenges Facing Water Resources and Sustainable Development of Wadi Feiran Basin, Southern Sinai, Egypt." *Hydrogeology Journal* 26, no. 7: 2475–2493.
- Ajibade, F. O., T. F. Ajibade, T. E. Idowu, et al. 2021. "Flood-Prone Area Mapping Using GIS-Based Analytical Hierarchy Frameworks for Ibadan City, Nigeria." *Journal of Multi-Criteria Decision Analysis* 28, no. 5–6: 283–295. <https://doi.org/10.1002/mcda.1759>.
- Alarifi, S. S., M. Abdelkareem, F. Abdalla, and M. Alotaibi. 2022. "Flash Flood Hazard Mapping Using Remote Sensing and GIS Techniques in Southwestern Saudi Arabia." *Sustainability* 14, no. 21: 14145. <https://doi.org/10.3390/su14211414>.
- Ali, S. A., F. Parvin, Q. B. Pham, et al. 2020. "GIS-Based Comparative Assessment of Flood Susceptibility Mapping Using Hybrid Multi-Criteria Decision-Making Approach, Naïve Bayes Tree, Bivariate Statistics, and Logistic Regression: A Case of Topľa Basin, Slovakia." *Ecological Indicators* 117: 106620. <https://doi.org/10.1016/j.ecolind.2020.106620>.
- Ali, Z., N. Dahri, M. Vanclooster, et al. 2023. "Hybrid Fuzzy AHP and Frequency Ratio Methods for Assessing Flood Susceptibility in Bayech Basin, Southwestern Tunisia." *Sustainability* 15, no. 21: 15422. <https://doi.org/10.3390/su152115422>.
- Allafta, H., and C. Opp. 2021. "GIS-Based Multi-Criteria Analysis for Flood Prone Areas Mapping in the Trans-Boundary Shatt Al-Arab Basin, Iraq-Iran." *Geomatics, Natural Hazards and Risk* 12, no. 1: 2087–2116. <https://doi.org/10.1080/19475705.2021.1955755>.
- Al-Weshah, R. A. 2002. "Rainfall-Runoff Analysis and Modeling in Wadi Systems." In *Hydrology of Wadi Systems*, edited by H. Wheeler and R. A. Al Weshah, 87–111. UNESCO Publishing.
- Astutik, S., E. I. Pangastuti, E. A. Nurdin, et al. 2021. "Assessment of Flood Hazard Mapping Based on Analytical Hierarchy Process (AHP) and GIS: Application in Kencong District, Jember Regency, Indonesia." *Geosfera Indonesia* 6, no. 3: 353–376. <https://doi.org/10.19184/geosi.v6i3.21668>.
- Aydin, M. C., and S. E. Birincioglu. 2022. "Flood Risk Analysis Using Gis-Based Analytical Hierarchy Process: A Case Study of Bitlis Province." *Applied Water Science* 12, no. 6: 122. <https://doi.org/10.1007/s13201-022-01655-x>.
- Barnett, V., and T. Lewis. 1984. *Outliers in Statistical Data*. Wiley.
- Berghout, A. 2025. Sensitivity of Flood-Prone Areas to Extreme Rainfall Using AHP and Fuzzy AHP: A Case Study of Boussellam and K'sob Watersheds, Algeria Sensitivity of Flood-Prone Areas to Extreme Rainfall Using AHP and Fuzzy AHP: A Case Study of Boussellam and K'sob Watersheds, Algeria. <https://doi.org/10.2166/wcc.2025.520>.
- Binns, A. D. 2022. "Sustainable Development and Flood Risk Management." *Journal of Flood Risk Management* 15, no. 2: e12807. <https://doi.org/10.1111/jfr3.12807>.
- Bokhari, B. F., B. Tawabini, and H. M. Baalousha. 2024. "A Fuzzy Analytical Hierarchy Process -GIS Approach to Flood Susceptibility Mapping in NEOM, Saudi Arabia." *Frontiers in Water* 6: 1388003. <https://doi.org/10.3389/frwa.2024.1388003>.
- Dang, N. M., and L. Kumar. 2017. "Application of Remote Sensing and GIS for Flood Risk Mapping: A Case Study in Vietnam." *Hydrology* 4, no. 3: 41. <https://doi.org/10.3390/hydrology4030041>.
- Das, S., and A. Gupta. 2021. "Multi-Criteria Decision Based Geospatial Mapping of Flood Susceptibility and Temporal Hydro-Geomorphical Changes in the Subarnarekha Basin, India." *Geoscience Frontiers* 12: 101206. <https://doi.org/10.1016/j.gsf.2021.101206>.
- Demir, V., and O. Kisi. 2016. "Flood Hazard Mapping by Using Geographic Information System and Hydraulic Model: Mert River, Samsun, Turkey." *Advances in Meteorology* 2016: 4891015. <https://doi.org/10.1155/2016/4891015>.
- Desalegn, H., and A. Mulu. 2021. "Flood Vulnerability Assessment Using GIS at Fetam Watershed, Upper Abbay Basin, Ethiopia." *Heliyon* 7, no. 1: e05865. <https://doi.org/10.1016/j.heliyon.2020.e05865>.
- Dhawaskar, P. 2015. "Morphometric Analysis of Mhadei River Basin Using SRTM Data and GIS." *SIJ Transactions on Advances in Space Research and Earth Exploration* 1, no. 4: 1–7.
- EEAA. 2005. South Sinai Government Environment Profile. SEAM Program, Egyptian Environment Affairs Agency (EEAA), Egypt.
- Elsadek, W. M., and A. H. Almaliki. 2024. "Integrated Hydrological Study for Flash Flood Assessment Using Morphometric Analysis and MCDA Based on Hydrological Indices—Al-Sail Al-Kabir, KSA." *Natural Hazards* 120, no. 7: 6853–6880. <https://doi.org/10.1007/s11069-024-06450-2>.
- Elsaid, K., M. Elshemy, and A. Negm. 2023. "Flood Susceptibility Mapping Using Ensemble Machine Learning Models: Case Study in Egypt." *Natural Hazards* 118, no. 2: 1789–1810. <https://doi.org/10.1007/s11069-023-06127-3>.
- Elsheikh, A. E., M. A. El Ammawy, N. M. Hamadallah, S. H. A. Hassan, and M. H. Darwish. 2024. "The Surface Water Potentiality in Arid and Semi-Arid Basins Using GIS and HEC-HMS Modeling, Case Study: Gebel El Sibai Watershed, Red Sea." *Water* 16, no. 21: 3111.
- Farhadi, S., and M. Najafzadeh. 2021. "Flood Susceptibility Assessment Using Machine Learning Models." *Environmental Earth Sciences* 80, no. 2: 1–19. <https://doi.org/10.1007/s12665-021-09315-8>.
- Ghanem, M. A. A. N., and H. Zaifoglu. 2024. "A Geospatial Analysis of Flood Risk Zones in Cyprus: Insights From Statistical and Multi-Criteria Decision Analysis Methods." *Environmental Science and Pollution Research* 31, no. 22: 32875–32900. <https://doi.org/10.1007/s11356-024-33391-x>.
- Hagos, Y. G., T. G. Andualem, M. Yibeltal, and M. A. Mengie. 2022. "Flood Hazard Assessment and Mapping Using GIS Integrated With Multi-Criteria Decision Analysis in Upper Awash River Basin, Ethiopia." *Applied Water Science* 12, no. 2: 1–18. <https://doi.org/10.1007/s13201-022-01674-8>.
- Hawkins, D. M. 1980. *Identification of Outliers*. Vol. 11. Chapman and Hall.
- Hegazi, A. M., and I. H. E. Bagouri. 2011. National Action Plan. Arab Republic of Egypt, Cairo.
- Hermas, E., S. Leprince, and I. A. El-Magd. 2012. "Retrieving Sand Dune Movements Using Sub-Pixel Correlation of Multi-Temporal Optical Remote Sensing Imagery, Northwest Sinai Peninsula, Egypt." *Remote Sensing of Environment* 121: 51–60.
- Hong, H., M. Panahi, A. Shirzadi, et al. 2018. "Flood Susceptibility Assessment in Hengfeng Area Coupling Adaptive Neuro-Fuzzy Inference System With Genetic Algorithm and Differential Evolution." *Science of the Total Environment* 621: 1124–1141. <https://doi.org/10.1016/j.scitotenv.2017.10.114>.
- Hong, H., P. Tsangaratos, I. Ilia, J. Liu, A.-X. Zhu, and W. Chen. 2018. "Application of Fuzzy Weight of Evidence and Data Mining Techniques in Construction of Flood Susceptibility Map of Poyang County, China." *Science of the Total Environment* 625: 575–588. <https://doi.org/10.1016/j.scitotenv.2017.12.256>.
- Ibrahim, A. S., I. S. Al Zayed, F. S. Abdelhaleem, M. M. Afify, A. Ahmed, and I. Abd-Elaty. 2023. "Identifying Cost-Effective Locations of Storage Dams for Rainfall Harvesting and Flash Flood Mitigation in Arid and Semi-Arid Regions." *Journal of Hydrology: Regional Studies* 50: 101526.

- Ibrahim, K. T. 2004. *Water Resources Management for Wadi WATIR (South Sinai)* (Unpublished Master Dissertation). Ain Shams University.
- Kanani-Sadat, Y., R. Arabsheibani, F. Karimipour, and M. A. Nasser. 2019. "A New Approach to Flood Susceptibility Assessment in Data-Scarce and Ungauged Regions Based on a GIS-Based Hybrid Multi-Criteria Decision-Making Method." *Journal of Hydrology* 572: 17–31. <https://doi.org/10.1016/j.jhydrol.2019.02.048>.
- Karymbalis, E., M. Andreou, D.-V. Batzakis, K. Tsanakas, and S. Karalis. 2021. "Integration of GIS-Based Multicriteria Decision Analysis and Analytic Hierarchy Process for Flood-Hazard Assessment in the Megalo Rema River Catchment (East Attica, Greece)." *Sustainability* 13, no. 18: 10232. <https://doi.org/10.3390/su131810232>.
- Lahmer, T. M., S. V. Kumar, and K. A. Locke. 2023. "Interconnected Hydrologic Extreme Drivers and Impacts Depicted by Remote Sensing Data Assimilation." *Scientific Reports* 13: 3411. <https://doi.org/10.1038/s41598-023-30484-4>.
- Lalbiakmawia, F. 2015. "Application of Remote Sensing and GIS Techniques for Ground Water Potential Zones Mapping in Aizawl District, Mizoram, India." *International Journal of Engineering Science and Research Technology* 4, no. 1: 292–300.
- Landis, J. R., and G. G. Koch. 1977. "The Measurement of Observer Agreement for Categorical Data." *Biometrics* 33, no. 1: 159–174. <https://doi.org/10.2307/2529310>.
- Lee, S., and F. Rezaie. 2022. "Data Used for GIS-Based Flood Susceptibility Mapping." *Geo Data* 41: 1–15. <https://doi.org/10.22761/DJ2022.4.1.001>.
- Maher, M., T. H. Nasrallah, M. Rabah, and F. S. Abdelhaleem. 2022. "Watershed Delineation and Runoff Estimation of Wadi Tayyibah, South Sinai Using Arc-GIS and HEC-HMS Model." *Port-Said Engineering Research Journal* 26, no. 2: 61–71. <https://doi.org/10.21608/pserj.2022.111930.1155>.
- Mahmoud, S. H., and T. Y. Gan. 2018. "Multi-Criteria Approach to Develop Flood Susceptibility Maps in Arid Regions of Middle East." *Journal of Cleaner Production* 196: 216–229. <https://doi.org/10.1016/j.jclepro.2018.06.047>.
- Meshram, S. A., and S. P. Khadse. 2015. "Morphometric Analysis of Madurai Basin—A Case Study of Cauvery Sub Watershed Region of Tamil Nadu, India." *International Journal of Advanced Engineering Research and Development* 3, no. 2: 23–32.
- Moore, I. D., R. B. Grayson, and A. R. Ladson. 1991. "Digital Terrain Modeling: A Review of Hydrological, Geomorphological, and Biological Applications." *Hydrometallurgy and Process Metallurgy* 5: 3–30.
- Ozkan, S. P., and C. Tarhan. 2016. "Detection of Flood Hazard in Urban Areas Using GIS: Izmir Case." *Procedia Technology* 22: 373–381. <https://doi.org/10.1016/j.protcy.2016.01.088>.
- Rahmati, O., H. Zeinivand, and M. Besharat. 2015. "Flood Hazard Zoning in Yasooj Region, Iran, Using GIS and Multi-Criteria Decision Analysis." *Geomatics, Natural Hazards and Risk* 7, no. 3: 1000–1017. <https://doi.org/10.1080/19475705.2015.1045043>.
- Razavi-Termeh, S. V., A. Kornejady, H. R. Pourghasemi, and S. D. Keesstra. 2018. "Flood Susceptibility Mapping Using Novel Ensembles of Adaptive Neuro-Fuzzy Inference System and Meta-Heuristic Algorithms." *Science of the Total Environment* 615: 438–451. <https://doi.org/10.1016/j.scitotenv.2017.09.262>.
- Rebouch, N., F. Tout, H. Dinar, Y. Benzid1, and Z. Zouak. 2024. "Integrating Multi-Source Geospatial Data and AHP for Flood Susceptibility Mapping in Ain Smara, Constantine, Algeria." *International Journal of Disaster Risk Management* 6, no. 2: 245–264. <https://doi.org/10.18485/ijdrm.2024.6.2.16>.
- Saaty, T. L. 2008. "Decision Making With the Analytic Hierarchy Process." *International Journal of Services Sciences* 1, no. 1: 83–98.
- Saaty, W. A. 1987. "The Analytic Hierarchy Process-What and How It Is Used." *Mathematical Modelling* 9, no. 3–5: 161–176.
- Satheeshkumar, S., S. Venkateswaran, and R. Kannan. 2017. "Rainfall–Runoff Estimation Using SCS–CN and GIS Approach in the Pappiredipatti Watershed of the Vaniyar Sub Basin, South India." *Modeling Earth Systems and Environment* 3, no. 1: 1–8. <https://doi.org/10.1007/s40808-017-0301-4>.
- Shultz, M. J. 2007. Comparison of Distributed Versus Lumped Hydrologic Simulation Models Using Stationary and Moving Storm Events Applied to Small Synthetic Rectangular Basins and an Actual Watershed Basin (Ph.D. Degree). The University of Texas.
- Tehrany, M. S., B. Pradhan, and M. N. Jebur. 2017. "Spatial Prediction of Susceptible Areas Using Rule-Based Decision Tree (DT) and a Novel Ensemble Bivariate and Multivariate Statistical Models in GIS." *Journal of Hydrology* 550: 558–575. <https://doi.org/10.1016/j.jhydrol.2017.05.042>.
- USGS United States Geological Survey. 2020. Earthquake Lists, Maps, and Statistics. Accessed 18 March 2020. <https://www.usgs.gov/natural-hazards/earthquake-hazards/lists-maps-and-statistics>.
- Wang, Z., C. Lai, X. Chen, B. Yang, S. Zhao, and X. Bai. 2015. "Flood Hazard Risk Assessment Model Based on Random Forest." *Journal of Hydrology* 527: 1130–1141. <https://doi.org/10.1016/j.jhydrol.2015.06.008>.
- Zhao, G., B. Pang, Z. Xu, D. Peng, and L. Xu. 2018. "Assessment of Urban Flood Susceptibility Using Semi-Supervised Machine Learning Model." *Water* 10, no. 9: 1218. <https://doi.org/10.3390/w10091218>.
- Zhran, M., K. Ghanem, A. Tariq, et al. 2024. "Exploring a GIS-Based Analytic Hierarchy Process for Spatial Flood Risk Assessment in Egypt: A Case Study of the Damietta Branch." *Environmental Sciences Europe* 36, no. 1: 184. <https://doi.org/10.1186/s12302-024-01001-9>.
- Zzaman, R. U., S. Nowreen, M. Billah, and A. S. Islam. 2021. "Flood Hazard Mapping of Sangu River Basin in Bangladesh Using Multi-Criteria Analysis of Hydro Geomorphological Factors." *Journal of Flood Risk Management* 14, no. 3: e12715. <https://doi.org/10.1111/jfr3.12715>.

Appendix A

TABLE A1 | Types of data and their sources utilized for mapping flood-prone areas.

Data types	Data sources
DEM with 30 m spatial resolution	Downloaded from U.S. Geologic Survey (http://earthexplorer.usgs.gov/)
Digital Soil Map of wadi Ked	Downloaded from The World obtained from the Food and Agriculture Organization (FAO) website. (http://www.fao.org/geonetwork/srv/en/)
Digital Topographic Map of wadi Ked	The Water Resources Research Institute (WRII).
Sentinel 2 10 m spatial resolution Land Use/Land Cover (LULC) Map (2021)	Environmental System Research Institute (ESRI) (https://livingatlas.arcgis.com/landcover/)
Monthly Rainfall Data	The Water Resources Research Institute (WRII).
Highway Network	Open Street Map (OSM) Website.
Sentinel 2A satellite image with 10 m spatial resolution	Downloaded from U.S. Geologic Survey (http://earthexplorer.usgs.gov/)

TABLE A2 | Saaty's preference scale (T. L. Saaty 2008).

Significance of importance top of form bottom of form	Definition
1	Equal significance
3	Moderate significance top of form bottom of form
5	Strong significance
7	Very strong or proven significance
9	Extreme significance
2, 4, 6, 8	Intermediate values

TABLE A3 | The random index (RI) is utilized to calculate the consistency ratio (CR) (W. A. Saaty 1987).

<i>n</i>	1	2	3	4	5	6	7	8	9	10	11	12	13	14	15
RI	0	0	0.58	0.9	1.12	1.24	1.32	1.41	1.45	1.49	1.51	1.53	1.56	1.57	1.59

TABLE A4 | Rainfall depths and areas of wadi Ked for different return periods.

Rainfall station	Return period (years)		Area (km ²)
	<i>R_p</i> (50 years)	<i>R_p</i> (100 years)	
Dahab	67.6	79.1	352.9
Sant Chatherine	72.3	85.0	421.3
Sharm Sheikh	49.6	58.1	282.4
Wadi Ked	64.7	75.8	1056.6

TABLE A5 | Factors influencing flooding, their categories, rating values, area coverage, and percentage.

<i>n</i>	Factor	Unit	Class	Ratings	Flood susceptibility class ratings	Weighting (%)	Area (km ²)	(%)
1	Elevation (E)	m	0–466	5	Very high	17	171.39	16%
			466.1–797	4	High		275.26	26%
			797.1–1133	3	Moderate		273.73	26%
			1134–1500	2	Low		223.22	21%
			1501–2421	1	Very low		113.01	11%
2	Slope (S)	—	0–10	5	Very high	16	188.27	18%
			11.0–20	4	High		252.49	24%
			21–28	3	Moderate		295.60	28%
			29–37	2	Low		237.92	23%
			38–74	1	Very low		82.27	8%
3	Rainfall (R)	mm/year	36–40	1	Very low	13	190.84	18%
			41–44	2	Low		182.09	17%
			45–47	3	Moderate		197.31	19%
			48–49	4	High		297.25	28%
			50–53	5	Very high		189.07	18%
4	Distance to streams (DS)	m	300	5	Very high	12	115.84	11%
			600	4	High		103.60	10%
			900	3	Moderate		93.79	9%
			1200	2	Low		86.33	8%
			> 2000	1	Very low		657.22	62%
5	Distance from roads (DR)	Data Geol Ecol Oceanogr Space Sci Polar Sci	0–1740	5	high	12	453.98	43%
		Data Geol Ecol Oceanogr Space Sci Polar Sci	1750–4090	4	High		238.09	23%
		Data Geol Ecol Oceanogr Space Sci Polar Sci	4100–6970	3	Moderate		174.73	17%
		Data Geol Ecol Oceanogr Space Sci Polar Sci	6980–10,600	2	Low		112.31	11%
		Data Geol Ecol Oceanogr Space Sci Polar Sci	10, 700–17, 100	1	Very low		77.14	7%
6	Drainage density (DD)	m/km	0.162–1.93	1	Very low	8	244.74	23%
			1.94–3.01	2	Low		279.15	26%
			3.02–4.12	3	Moderate		262.22	25%
			4.13–5.39	4	High		179.91	17%
			5.4–7.82	5	Very high		90.04	9%

(Continues)

TABLE A5 | (Continued)

<i>n</i>	Factor	Unit	Class	Ratings	Flood susceptibility class ratings	Weighting (%)	Area (km ²)	(%)
7	Topographic wetness index (TWI)	Level	2.2–5.2	1	Very low	6	452.72	43%
			5.2–6.9	2	Low		384.74	36%
			6.9–9.4	3	Moderate		151.35	14%
			9.4–13.7	4	High		51.46	5%
			13.7–24.3	5	Very high		15.39	1%
8	Land use/land cover (LULC)	Level	Water	5	Very high	7	0.02	0%
			Scrub/shrub	2	Low		139.23	13%
			Bare Ground	4	High		917.34	87%
9	Normalized Difference Vegetation Index (NDVI)	Level	−0.264 to −0.0113	5	Very high	3	79.83	8%
			−0.0112 to 0.00856	4	High		216.81	21%
			0.00857–0.0259	3	Moderate		316.03	30%
			0.026–0.0433	2	Low		279.98	26%
			0.0434–0.368	1	Very low		162.89	15%
10	Curvature (C)	Level	−31.6 to 1.31	4	High	2	118.85	11%
			−1.3 to 0.756	5	Very high		703.52	67%
			0.757–34.4	3	Moderate		234.16	22%
11	Soil type (ST)	Level	Lithosols	2	Low	4	904.37	86%
			Eutric Regosols	3	Moderate		149.22	14%

TABLE A6 | Comparison between the questionnaire matrix and matrix from this study.

	This study	Questionnaire
λ_{\max}	11.789	11.9926
CI	0.079	0.0993
RI	1.510	1.5100
CR	0.052	0.0657

TABLE A7 | Cross-tabulated susceptibility class distributions and probabilities for literature-based and expert-based AHP maps used in Kappa coefficient calculation.

Susceptibility class	No. Map1 cells (literature-based)	No. Map2 cells (Expert-based)	Matched cells	Probability of Map1 (p_1)	Probability of Map2 (p_2)	$p_1 \times p_2$
Very low (1)	280	282	280	0.01184	0.01193	0.00014
Low (2)	6276	6205	6205	0.26548	0.26248	0.06968
Moderate (3)	10,501	10,507	10,501	0.44420	0.44446	0.19743
High (4)	6216	6284	6216	0.26294	0.26582	0.06990
Very High (5)	367	362	362	0.01552	0.01531	0.00024

TABLE A8 | Interpretation scale of Cohen's Kappa coefficient according to Landis and Koch (1977).

Kappa value	Interpretation
<0.00	Poor agreement
0.00–0.20	Slight agreement
0.21–0.40	Fair agreement
0.41–0.60	Moderate agreement
0.61–0.80	Substantial agreement
0.81–1.00	Almost perfect agreement

TABLE A9 | Rainfall data screening for rainfall stations.

Station	Available records	Number of records	K_n	High outlier	Low outlier	Max predicted rainfall	Min predicted rainfall	Result
Dahab	1981–2022	34	2.557	2.024	0.256	105.741	1.803	No outliers
Sant Chatherine	1981–2022	33	2.545	2.010	0.266	102.386	1.846	No outliers
Sharm Sheikh	1981–2022	27	2.459	1.813	0.211	64.940	1.626	No outliers

TABLE A10 | Curve number for sub-basins of Wadi Ked.

Sub basin no.		1	2	3	4	5	6	7	8	9
HSG	CN	Area (km ²)								
A	63	33.7	2.3	5.7	19.0	7.4	3.0	11.8	15.1	25.8
B	77	3.0	42.2	7.9	1.9	10.3	41.9	43.1	36.6	11.6
C	85	30.1	1.6	0.2	0.0	15.6	15.2	0.0	1.0	0.0
D	88	141.2	136.7	114.4	98.5	54.0	34.4	16.6	61.3	13.4
CN		84	86	87	84	85	82	78	82	73

TABLE A11 | The runoff volumes of sub-basins in Wadi Ked for various return periods.

Sub Basin	Potential maximum retention (S)	Longest Flow path Length (L) (Ft)	Basin slope (Y%)	Lag time (TL) (min)	Area (Km ²)	Curve Number (CN)	Return period (50year)		Return period (100year)	
							Peak discharge (m ³ /s)	Volume (MCM)	Peak discharge (m ³ /s)	Volume (MCM)
1	1.90	91537.60	43.23	94.40	208.2	84	464.6	6.57	611.1	8.52
2	1.63	101024.64	47.69	90.67	182.9	86	474.1	6.39	611.4	8.18
3	1.49	94583.69	49.75	81.19	128.2	87	377.9	4.71	483.8	5.99
4	1.90	78464.37	45.85	81.03	71.5	84	177.6	2.25	233.7	2.92
5	1.76	76109.81	45.55	76.64	94.6	85	261.2	3.14	339.7	4.05
6	2.20	68248.23	42.84	80.15	87.3	82	193.6	2.48	259.7	3.26
7	2.82	102249.34	43.52	124.54	119.4	78	148.7	2.71	207.2	3.67
8	2.20	68228.38	34.55	89.23	113.5	82	235	3.22	314.6	4.24
9	3.70	63864.44	18.13	153.05	34.4	73	25.2	0.57	37.3	0.81

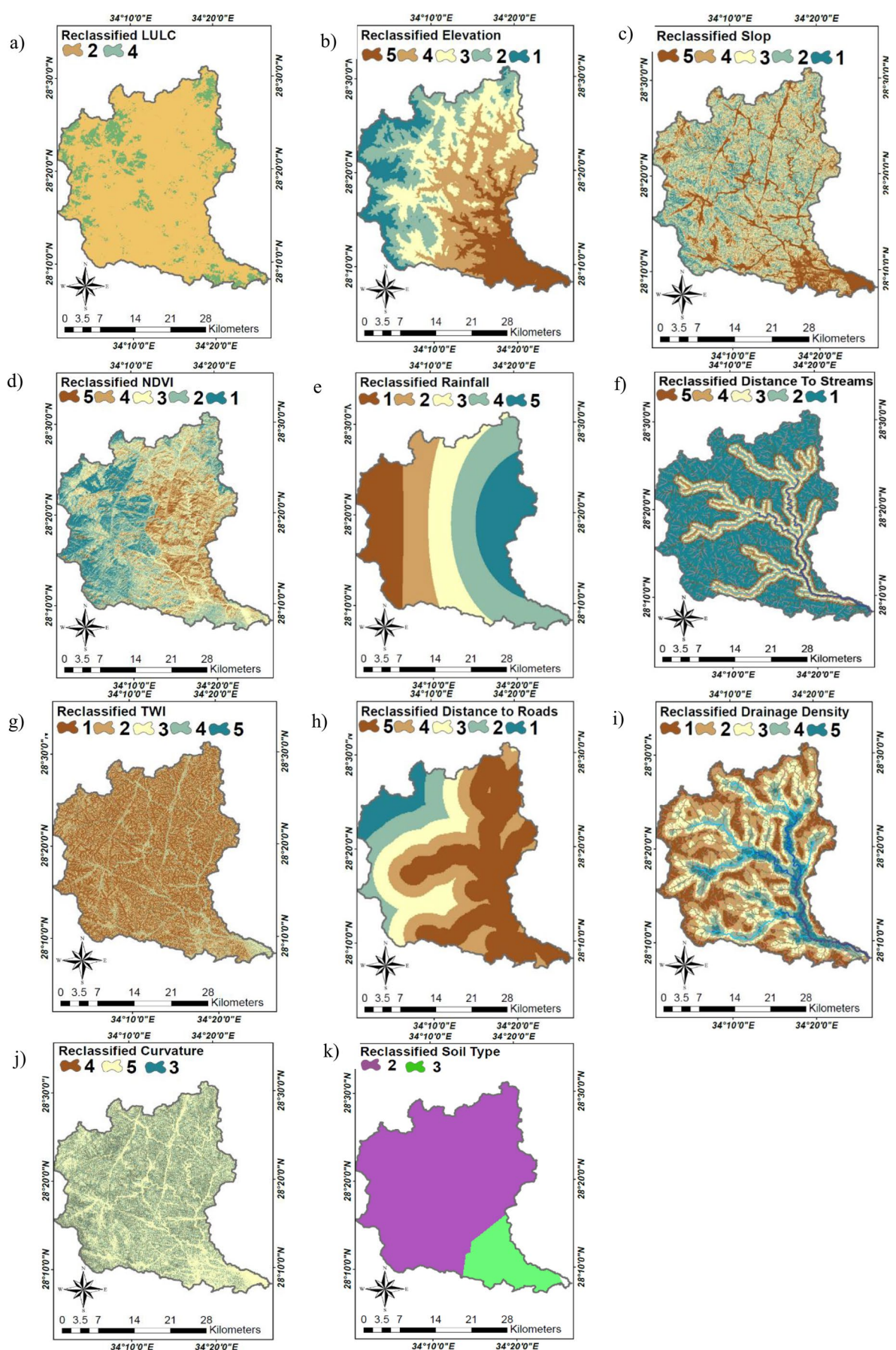


FIGURE A1 | Wadi Ked for (a) LULC, (b) elevation, (c) slope, (d) NDVI, (e) Rainfall (f) DS, (g) TWI, (h) DR, (i) DD, (j) curvature, and (k) soil type.